The state-of-the-art in cardiac MRI reconstruction

Results of the CMRxRecon challenge in MICCAI 2023

Lyu, Jun; Qin, Chen; Zhao, Yidong; Tao, Qian; Wu, Lianming; Yang, Guang; Qu, Xiaobo; Wang, He; Wang, Chengyan; More Authors

DOI
10.1016/j.media.2025.103485

Publication date
2025

Document Version
Final published version

Published in
Medical Image Analysis

Citation (APA)
Lyu, J., Qin, C., Zhao, Y., Tao, Q., Wu, L., Yang, G., Qu, X., Wang, H., Wang, C., & More Authors (2025). The state-of-the-art in cardiac MRI reconstruction: Results of the CMRxRecon challenge in MICCAI 2023. *Medical Image Analysis*, *101*, Article 103485. https://doi.org/10.1016/j.media.2025.103485

Medical Image Analysis 101 (2025) 103485

Contents lists available at ScienceDirect

Medical Image Analysis

journal homepage: www.elsevier.com/locate/media

The state-of-the-art in cardiac MRI reconstruction: Results of the CMRxRecon challenge in MICCAI 2023

Jun Lyu [1,a], Chen Qin [2,a], Shuo Wang [3,a], Fanwen Wang [4,5,a], Yan Li [7], Zi Wang [8,4], Kunyuan Guo [8], Cheng Ouyang [9,10], Michael Tänzer [9,5], Meng Liu [11,13], Longyu Sun [11,13], Mengting Sun [11,13], Qing Li [11,13], Zhang Shi [14], Sha Hua [15], Hao Li [16], Zhensen Chen [16], Zhenlin Zhang [2], Bingyu Xin [17], Dimitris N. Metaxas [17], George Yiasemis [18], Jonas Teuwen [18], Liping Zhang [19], Weitian Chen [19], Yidong Zhao [20], Qian Tao [20], Yanwei Pang [21], Xiaohan Liu [22], Artem Razumov [23], Dmitry V. Dylov [23,37], Quan Dou [24], Kang Yan [24], Yuyang Xue [25], Yuning Du [25], Julia Dietlmeier [26], Carles Garcia-Cabrera [27], Ziad Al-Haj Hemidi [28], Nora Vogt [29], Ziqiang Xu [30], Yajing Zhang [31], Ying-Hua Chu [32], Weibo Chen [33], Wenjia Bai [9,10], Xiahai Zhuang [34], Jing Qin [35], Lianming Wu [36,*], Guang Yang [4,5,6,*], Xiaobo Qu [8,*], He Wang [12,16,*], Chengyan Wang [11,13,*]

[1] School of Computer and Control Engineering, Yantai University, Yantai, China
[2] Department of Electrical and Electronic Engineering & I-X, Imperial College London, United Kingdom
[3] Digital Medical Research Center, School of Basic Medical Sciences, Fudan University, Shanghai, China
[4] Department of Bioengineering & Imperial-X, Imperial College London, London W12 7SL, UK
[5] Cardiovascular Magnetic Resonance Unit, Royal Brompton Hospital, Guy's and St Thomas' NHS Foundation Trust, London SW3 6NP, UK
[6] School of Biomedical Engineering & Imaging Sciences, King's College London, London WC2R 2LS, UK
[7] Department of Radiology, Ruijin Hospital, Shanghai Jiao Tong University School of Medicine, Shanghai, China
[8] Department of Electronic Science, Fujian Provincial Key Laboratory of Plasma and Magnetic Resonance, National Institute for Data Science in Health and Medicine, Institute of Artificial Intelligence, Xiamen University, Xiamen 361102, China
[9] Department of Computing, Imperial College London, London SW7 2AZ, UK
[10] Department of Brain Sciences, Imperial College London, London SW7 2AZ, UK
[11] Shanghai Pudong Hospital and Human Phenome Institute, Fudan University, Shanghai, China
[12] Human Phenome Institute, Fudan University, 825 Zhangheng Road, Pudong New District, Shanghai, 201203, China
[13] International Human Phenome Institute (Shanghai), Shanghai, China
[14] Department of Radiology, Zhongshan Hospital, Fudan University, Shanghai, China
[15] Department of Cardiovascular Medicine, Ruijin Hospital Lu Wan Branch, Shanghai Jiao Tong University School of Medicine, Shanghai, China
[16] Institute of Science and Technology for Brain-Inspired Intelligence, Fudan University, Shanghai, 200433, China
[17] Department of Computer Science, Rutgers University, New Brunswick, NJ 08901, USA
[18] AI for Oncology, Netherlands Cancer Institute, Plesmanlaan 121, 1066 CX, Amsterdam, Netherlands
[19] CUHK Lab of AI in Radiology (CLAIR), Department of Imaging and Interventional Radiology, The Chinese University of Hong Kong, China
[20] Department of Imaging Physics, Delft University of Technology, Lorentzweg 1, 2628CN, Delft, Netherlands
[21] TJK-BIIT Lab, School of Electrical and Information Engineering, Tianjin University, Tianjin 300072, China
[22] Institute of Applied Physics and Computational Mathematics, Beijing, 100094, China
[23] Skolkovo Institute Of Science And Technology, Center for Artificial Intelligence Technology, 30/1 Bolshoy blvd., 121205 Moscow, Russia
[24] Department of Biomedical Engineering, University of Virginia, 415 Lane Rd., Charlottesville, VA 22903, United States
[25] Institute for Imaging, Data and Communications, University of Edinburgh, EH9 3FG, UK
[26] Insight SFI Research Centre for Data Analytics, Dublin City University, Glasnevin Dublin 9, Ireland
[27] ML-Labs SFI Centre for Research Training in Machine Learning, Dublin City University, Glasnevin Dublin 9, Ireland
[28] Institute of Medical Informatics, Universität zu Lübeck, Ratzeburger Alle 160, 23562 Lübeck, Germany
[29] IADI, INSERM U1254, Université de Lorraine, Rue du Morvan, 54511 Nancy, France
[30] School of Health Science and Engineering, University of Shanghai for Science and Technology, Shanghai, China
[31] Science & Technology Organization, GE Healthcare, Beijing, China
[32] Siemens Healthineers Ltd., China
[33] Philips Healthcare, Shanghai, China

* Corresponding authors.
E-mail addresses: wulianming@shsmu.edu.cn (L. Wu), g.yang@imperial.ac.uk (G. Yang), quxiaobo@xmu.edu.cn (X. Qu), hewang@fudan.edu.cn (H. Wang), wangcy@fudan.edu.cn (C. Wang).
[a] These authors contribute equally.

https://doi.org/10.1016/j.media.2025.103485
Received 31 March 2024; Received in revised form 9 September 2024; Accepted 27 January 2025
Available online 6 February 2025

[34] School of Data Science, Fudan University, Shanghai, China
[35] School of Nursing, The Hong Kong Polytechnic University, Hong Kong, China
[36] Department of Radiology, Ren Ji Hospital, School of Medicine, Shanghai Jiao Tong University, Shanghai, 200127, China
[37] Artificial Intelligence Research Institute, 32/1 Kutuzovsky pr., Moscow, 121170, Russia

ARTICLE INFO

Keywords:
Reconstruction
Cardiac imaging
Fast imaging
Under-sampling
K-space

ABSTRACT

Cardiac magnetic resonance imaging (MRI) provides detailed and quantitative evaluation of the heart's structure, function, and tissue characteristics with high-resolution spatial–temporal imaging. However, its slow imaging speed and motion artifacts are notable limitations. Undersampling reconstruction, especially data-driven algorithms, has emerged as a promising solution to accelerate scans and enhance imaging performance using highly under-sampled data. Nevertheless, the scarcity of publicly available cardiac k-space datasets and evaluation platform hinder the development of data-driven reconstruction algorithms. To address this issue, we organized the Cardiac MRI Reconstruction Challenge (CMRxRecon) in 2023, in collaboration with the 26th International Conference on Medical Image Computing and Computer-Assisted Intervention (MICCAI). CMRxRecon presented an extensive k-space dataset comprising cine and mapping raw data, accompanied by detailed annotations of cardiac anatomical structures. With overwhelming participation, the challenge attracted more than 285 teams and over 600 participants. Among them, 22 teams successfully submitted Docker containers for the testing phase, with 7 teams submitted for both cine and mapping tasks. All teams use deep learning based approaches, indicating that deep learning has predominately become a promising solution for the problem. The first-place winner of both tasks utilizes the E2E-VarNet architecture as backbones. In contrast, U-Net is still the most popular backbone for both multi-coil and single-coil reconstructions. This paper provides a comprehensive overview of the challenge design, presents a summary of the submitted results, reviews the employed methods, and offers an in-depth discussion that aims to inspire future advancements in cardiac MRI reconstruction models. The summary emphasizes the effective strategies observed in Cardiac MRI reconstruction, including backbone architecture, loss function, pre-processing techniques, physical modeling, and model complexity, thereby providing valuable insights for further developments in this field.

1. Introduction

1.1. Background

Cardiac magnetic resonance imaging (MRI) has emerged as a crucial imaging technique for non-invasive diagnosis in clinical cardiology, due to its advantages in quantitative assessment of cardiac morphology and myocardial tissue characteristics (Eyre et al., 2022).

Cardiac cine (dynamic image sequence) offers a fine spatial and temporal resolution of the heart throughout the cardiac cycle. As the most common technique in cardiac MRI, cine can provide cardiac function measurements, e.g., cardiac output and ejection fraction (Menchón-Lara et al., 2019). In recent years, multi-contrast imaging methods, notably T1 mapping, and T2 mapping, have gained prominence in clinical applications (Qi et al., 2021). These mapping techniques exhibit high sensitivity in detecting lesions, allowing for the quantitative assessment of myocardial fibrosis, hemorrhage, and edema (Jerosch-Herold and Coelho-Filho, 2022). In contrast to conventional methods, these techniques offer a direct measurement of the myocardial tissue's T1 and T2 attenuation values. These quantitative parameters can be utilized more effectively for the detection of diffuse lesions and provide a better benchmark for comparing measurements across multiple centers. Although cardiac MRI offers numerous advantages, its main challenge lies in the slow scan speed it entails. Cine imaging captures multiple phases using segmented acquisition spread over different heartbeats, while mapping techniques require sampling multiple frames across the magnetization recovery to estimate T1 and T2 values. To achieve comprehensive coverage of the heart, repeated acquisitions from different orientations result in extended imaging time. This slow speed not only compromises the image quality due to the accumulation of imaging artifacts caused by patient movement but also exacerbates patient discomfort during the scanning process. To expedite cardiac MRI, the current accelerated solution involves compressed sensing (CS) (Donoho, 2006; Lustig et al., 2008). Instead of sampling the entire MRI signal space (Fourier space, usually termed as *k-space*), CS only acquires a subset of k-space and recovers these sub-Nyquist measurements using iterative reconstruction algorithms. However, CS-MRI reconstructions have limited acceleration factors in practical use, and the introduction of certain regularization terms can compromise the fidelity and clarity of the resulting images. Additionally, the CS algorithm often requires prolonged computation time due to its iterative nature (Lustig et al., 2008; Uecker et al., 2014). Therefore, the accurate and robust reconstruction of multi-contrast cardiac images from highly undersampled k-space data remains an open problem.

In recent years, data-driven methods (Lyu et al., 2022, 2023b,c; Lv et al., 2021a,b,c, 2020, 2018) have reshaped the general practice of image reconstruction. In addition to innovative network designs, the performance of these algorithms largely depends on the size and quality of the training dataset. To this end, several large-scale challenges, such as fastMRI (Zbontar et al., 2018) and MC-MRI (Beauferris et al., 2022), have been organized for fair evaluations of these reconstruction algorithms. To date, there have been no dedicated challenges or publicly available datasets specifically focused on cardiac MRI reconstruction, not to mention the absence of a comprehensive and fair evaluation benchmark for the development of deep learning-enabled cardiac MRI reconstructions.

1.2. Challenges of cardiac MRI reconstruction

Cardiac MRI reconstruction faces several prominent challenges, including:

- Variable heart rhythms: Patients may have variable heart rates, leading to variations in the duration of cardiac cycles. This variability can impact the synchronization of data acquisition, requiring adaptive reconstruction methods to handle different heart rates effectively.
- Motion artifacts: The heart is a dynamic organ that undergoes continuous motion during the cardiac cycle resulting from inconsistencies across different segments of the acquisition process. Similarly, cardiac motion, as well as respiratory motion, may induce blurring in the reconstructed images, particularly when the acquisition window encompasses phases of rapid movement (Ismail et al., 2022).

- Complex anatomy: The intricate anatomy of the heart, including delicate structures and complex geometries, requires reconstruction algorithms capable of preserving spatial details and accurately representing cardiac structures. On the other hand, if the training samples do not include certain diseases present in the test set, it can lead to a significant performance drop in deep-learning reconstruction models.
- Limited temporal resolution: Cardiac MRI involves capturing images at different phases of the cardiac cycle. Limited temporal resolution can result in inadequate coverage of dynamic events within the heart, which needs to be improved by accelerating the imaging and reducing the acquisition window.
- Integration of deep learning with conventional methods: Technical solutions are still needed to effectively integrate conventional parallel imaging with deep learning techniques to maximize their respective advantages.
- High demands on computational resources: The raw data acquired during cardiac MRI scans, often coupled with the need for real-time reconstruction in some cases, poses significant computational challenges. Efficient algorithms and powerful hardware are essential for timely reconstruction.

There have been continuous efforts to develop advanced image reconstruction techniques, from compressed sensing to deep learning approaches, to address these challenges and improve the overall quality and efficiency of cardiac MRI reconstruction. The outcome of these advancements will be expected to contribute to more accurate diagnoses and better patient outcomes in cardiac imaging.

1.3. Limitation of existing datasets

To date, NYU Langone Health has released the "fastMRI" dataset, containing the multi-coil brain, knee, and prostate MRI raw k-space data. Similarly, the Universities of Calgary and Campinas have provided the MRI community with the "Calgary-Campinas" dataset (Souza et al., 2018), comprising multi-coil brain acquisitions. However, these datasets do not apply to the spatio-temporal scenario in cardiac imaging. To the best of our knowledge, previous available cardiac raw datasets mainly include OCMR (Chen et al., 2020) and Harvard CMR Dataverse (El-Rewaidy et al., 2022). The former provides fully sampled cine data as well as prospectively undersampled data, while the latter also offers cine data with radial sampling trajectories, including 101 patients and 7 healthy volunteers. However, these datasets suffer from limitations in a lack of anatomical views, imaging contrasts, and size of the dataset. In comparison, our CMRxRecon dataset aims to provide a larger data size (300 subjects), more imaging contrasts (cine, T1 mapping, T2 mapping), and more anatomical views (short-axis, 2/3/4-chambers). Additionally, the CMRxRecon dataset is currently the only publicly released cardiac MRI reconstruction dataset associated with an open challenge.

1.4. CMRxRecon challenge

CMRxRecon challenge is jointly organized by 10 institutions: Fudan University, Imperial College London, Hong Kong Polytechnic University, Xiamen University, the University of Texas, Shanghai Polytechnic University, Shanghai Jiao Tong University, Fudan University Affiliated Zhongshan Hospital, and Siemens Healthineers. It is a one-time event with fixed submission deadline. The CMRxRecon challenge aims to establish a platform for fast cardiac MRI reconstruction and provide a benchmark dataset that enables the broad research community to promote advances in this area of research, which includes two independent tasks:

- Accelerated cine reconstruction

The aim of task 1 is to accelerate cine imaging from under-sampling data and address the image degradation problem caused by k-space under-sampling.

- Accelerated T1 & T2 mapping

The aim of task 2 is to improve the T1 and T2 mapping from under-sampling data and address the image degradation problem caused by k-space under-sampling.

1.5. Challenge rules

Each team can choose to participate one of them or both. The top 3 winners in each task are invited to give oral presentations during the 26th International Conference on Medical Image Computing and Computer Assisted Intervention (MICCAI). The recommended authors of the top 3 winner teams are invited to contribute to the challenge summary paper. In addition, monetary awards are provided for the top 3 winners of each task. The prize pool is exclusively sponsored by Siemens Healthineers. Members of the organizers' institutes can participate but are not eligible for awards. Participating teams can publish their own results separately after the embargo time (three months after the announcement of the final results).

1.6. Contributions

The contributions of the "CMRxRecon" challenge include but are not limited to the following aspects:

- Open dataset: CMRxRecon is the first cardiac MRI reconstruction challenge that provides an open dataset consisting of multi-contrast, multi-view, and multi-coil raw k-space data from 300 subjects with complete cardiac segmentation labels. This rich dataset holds crucial value for the development of deep learning algorithms.
- Evaluation platform: Our challenge provides a benchmarking platform that enables timely evaluation of reconstruction results. Researchers can conveniently compare different algorithms using the same data and the same assessment metrics, thereby expediting their research progress and facilitating future research in the cardiac MRI field.
- Methodology summary: Through the challenge, we evaluate and compare different deep-learning-based reconstruction methods on the two tasks, providing a summary of experiences and a comparison of the strengths and weaknesses of methods in the cardiac MRI reconstruction community. The summary highlights the effective strategies for CMR reconstruction, regarding the backbone architecture, loss function, pre-processing, physical model and model complexity, providing insights for further development.

In summary, the goal of establishing the CMRxRecon challenge is to provide a benchmark dataset that enables the broad research community to participate in this important work of accelerated CMR imaging. Through training and validation on this dataset using private models, we look forward to continuous technological breakthroughs in the field of cardiac MRI reconstruction, which will also contribute to the translation of the latest techniques into clinical practice.

2. Related work

2.1. Cardiac MRI challenges

Over the last decade, there have been several challenges that focused on cardiac MRI. The majority of them focus on the segmentation of anatomical structures of the heart, such as the left ventricle (LV), the myocardium (Myo), and the right ventricle (RV). For example, one of the earliest cardiac MRI segmentation challenges held by the

Cardiac Atlas Project (Suinesiaputra et al., 2014) required participants to segment the Myocardium on steady-state free precession (SSFP) cine in short-axis images. The Right Ventricle Segmentation Challenge (Petitjean et al., 2015) focused on the segmentation of the RV on cine. Subsequently, further related challenges emerged, including the Automated Cardiac Diagnosis Challenge (ACDC) (Bernard et al., 2018) and the Multi-Centre, Multi-Vendor and Multi-Disease Cardiac Image Segmentation Challenge (M&Ms) (Campello et al., 2021), which both consider the segmentation of LV, Myo and RV. The ACDC challenge is composed of 150 subjects divided into five subgroups (normal, myocardial infarction, dilated cardiomyopathy, hypertrophic cardiomyopathy, and abnormal right ventricle) and the M&Ms challenge additionally contributes to the effort of building generalizable models by providing CMR data scanned in clinical centers from three different countries using four different magnetic resonance scanner vendors, with a follow-up challenge on further incorporating multi-view CMR data (Martín-Isla et al., 2023). Beyond cine CMR, other CMR sequences have been explored for the segmentation tasks. For instance, the Multi-Sequence Cardiac MR Segmentation Challenge (MS-CMRSeg) (Zhuang et al., 2022) proposed to segment the ventricles and Myo using three CMR sequences, i.e. late gadolinium enhancement (LGE), T2 and bSSFP. The Atria Segmentation Challenge (Xiong et al., 2021) as well as the Left Atrial and Scar Quantification & Segmentation (LAScarQS) Challenge (Li et al., 2022) focused on the segmentation of left atrium and scar on LGE CMR. Whole heart segmentation has also been performed on both CT and MRI through the Multi-Modality Whole Heart Segmentation (MM-WHS) challenge (Zhuang et al., 2019).

Apart from the cardiac segmentation challenges, further challenges were held to tackle other CMR tasks, such as LV statistical shape modeling (Suinesiaputra et al., 2017) and classification of pathology (Bernard et al., 2018; Lalande et al., 2022). Cardiac motion has also been of great interest in the CMR community, and challenges such as on cardiac motion analysis (Tobon-Gomez et al., 2013) and motion correction (Pontré et al., 2016) have also been held. One recent challenge (CMRxMotion) (Wang et al., 2022b) has proposed to establish a public benchmark dataset to assess the effects of respiratory motion on CMR imaging quality and examine the robustness of automated segmentation models. Despite the numerous efforts to organize challenges and establish benchmarks for CMR analysis, no benchmarks for upstream CMR reconstruction applications have been proposed to date. Our effort in this work and challenge aims to establish a platform for fast CMR image reconstruction and provide a benchmark dataset with both dynamic cine CMR and quantitative T1/T2 mapping raw data, for promoting advances in this area of research.

2.2. Deep learning methods for cardiac MRI reconstruction

Deep learning (DL) approaches have gained great popularity for MRI reconstruction in recent years, due to their excellent capabilities in reconstructing high-quality MR images at fast reconstruction speed. Current deep learning methods for cardiac MRI reconstruction can generally be categorized into three types (Qin and Rueckert, 2022): image post-processing approaches, model-driven unrolled methods, and k-space-based interpolation techniques.

MRI reconstruction via image post-processing techniques typically learns an end-to-end mapping between zero-filled under-sampled images and ground truth fully-sampled references. Commonly, U-net architectures are employed to reduce image artifacts (Hauptmann et al., 2019; Kofler et al., 2019; Lyu et al., 2023c), where 3D convolutions or 2D convolutions on the spatio-temporal domain ($x-t$) are leveraged to exploit the temporal information of cardiac MRI sequences. However, one significant drawback of this type of approach is that they do not consider the physically acquired k-space raw data during the reconstruction process and thus cannot guarantee the consistency between the reconstructed images and the acquired signals. To improve on this, model-driven, unrolled approaches (Aggarwal et al., 2018; Hammernik et al., 2018; Qin et al., 2018; Schlemper et al., 2017; Duan et al., 2019; Wang et al., 2023b) have been proposed to embed the conventional iterative compressed sensing (CS)-based methods into deep learning frameworks. Such methods learn the unrolled optimization inspired by CS-based approaches, where the reconstruction process is alternated between a learnable image de-aliasing step parameterized by neural networks and a data consistency step. These models can be structured either in a cascaded fashion (Schlemper et al., 2017) or in a recurrent way (Qin et al., 2018) to mimic the iterative nature of the optimization-based approaches. This type of method has been shown to be able to achieve state-of-the-art performance in CMR reconstruction with high fidelity and good generalization capability (Hammernik et al., 2021), due to the incorporation of the physically acquired raw data within the learning process. Lastly, k-space interpolation approaches recover the missing data directly in k-space. For instance, CNNs or implicit neural representations can be used in k-space to learn the interpolation of k-space data given the auto-calibrating signals or the under-sampled signals (Akçakaya et al., 2019; Huang et al., 2023; Feng et al., 2022). These approaches are typically subject-specific and do not require training datasets, but will need separate training for each scan.

The recent advancement of DL in CMR reconstruction has mainly been developed based on the above three types of approaches while incorporating some more advanced DL techniques. For instance, transformers have been studied in the context of CMR reconstruction to exploit the spatio-temporal information within and across cardiac frames (Lyu et al., 2023a, 2024), and diffusion models have been investigated to leverage their generative power for recovering high-quality scans within the above three frameworks (Chung and Ye, 2022; Xie and Li, 2022; Güngör et al., 2023). A further research direction is to exploit information from complementary domains or use complementary regularization. For instance, regularization on spatial frequency domain along with that on image domain has been proposed to reconstruct the cine CMR (Qin et al., 2019, 2021), which has demonstrated better performance compared to single domain reconstruction. Similarly, there have also been works on joint k-space and image space reconstruction (Wang et al., 2022a), as well as reconstruction methods incorporating low-rank or sparse prior (Huang et al., 2021; Wang et al., 2024) or SmooThness regularization on manifolds (SToRM) prior (Biswas et al., 2019). Additionally, motion compensation on cine CMR has also been considered within the model-driven unrolled framework, where the reconstruction and motion are jointly estimated during the process (Seegoolam et al., 2019; Pan et al., 2024). For a more comprehensive review of the existing DL approaches for CMR reconstruction, please refer to Qin and Rueckert (2022).

Despite that the majority of the above-discussed DL methods focus on the cine CMR reconstruction, they should be generalizable to reconstruct each multi-contrast CMR in T1/T2 mapping. Alternatively, T1/T2 values can also be reconstructed directly without recovering each contrast image, such as using a fully connected neural network to predict the values directly (Guo et al., 2022). However, the current literature on CMR T1/T2 mapping reconstruction is limited, which could be explained by the lack of public CMR T1/T2 mapping datasets. Our effort in putting forward this CMRxRecon challenge with both cine and T1/T2 mapping CMR data will likely further strengthen the active research in the field.

3. Challenge setup

3.1. Dataset

3.1.1. Dataset information

Our institutional review board granted approval for the study (approval number: FE20017). Data collection was conducted using a 32-channel specialized cardiac coil in conjunction with a 3T scanner (MAGNETOM Vida, Siemens Healthineers, Germany). We successfully recruited and acquired data from 300 healthy volunteers at our medical

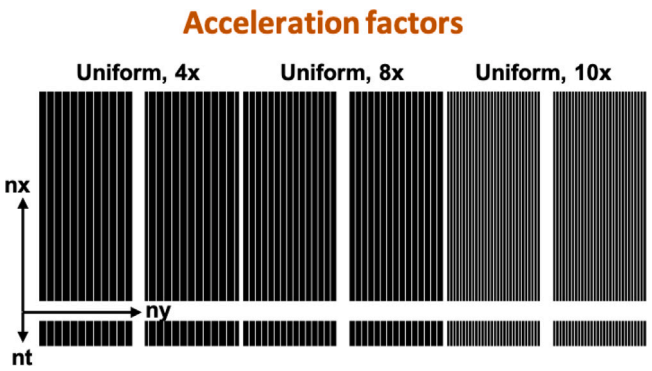

Fig. 1. The sampling masks under acceleration factors of 4, 8 and 10 with auto-calibration lines (ACS, 24 lines).

center. The data are divided into three sets, i.e., 120 training data, 60 validation data and 120 test data. Before the scans, participants were positioned in a supine posture. During the scan, electrodes were connected, and an electrocardiogram (ECG) signal was recorded. Cardiac Scout imaging was conducted using the 'Dot' engine. The CMRxRecon dataset (Wang et al., 2023a) follows the CC-BY license. All released data provided by the challenge is publicly available but limited to non-commercial use.

We followed the CMR imaging protocol given in the earlier publication (Wang et al., 2021). For 2D cardiac cine, the "TrueFISP" readout was employed. Long-axis (LAX) and short-axis (SAX), two-chamber (2CH), three-chamber (3CH), and four-chamber (4CH) views were gathered. Generally, 5 ∼ 11 slices were obtained for the SAX view while a single slice was obtained for each of the other views. Using a temporal resolution of around 50 ms, the cardiac cycle was divided into 12∼25 phases based on heart rate. Typical scan settings included an 8.0 mm slice thickness, a 1.5×1.5 mm^2 spatial resolution, a 3.6 ms repetition time (TR), and a 1.6 ms echo time (TE). The original acceleration factor for parallel imaging was R = 3. The signal was obtained with breath-holding.

Using a modified look-locker inversion recovery (MOLLI) sequence, nine images with various T1 weightings (using the 4-(1)-3-(1)-2 scheme) were obtained for T1 mapping. T1 mapping was performed only in SAX view, with a typical field-of-view (FOV) of 340×340 mm^2, spatial resolution of 1.5×1.5 mm^2, slice number of 5 or 6, slice thickness of 5.0 mm, TR of 2.7 ms, TE of 1.1 ms, partial Fourier of 6/8, and parallel imaging acceleration factor of R = 2. Subjects' inversion times differed based on their heart rates in real-time. Using an ECG trigger, signals were obtained after the diastole.

Using T2-prepared (T2prep)-FLASH sequence and three T2 weightings in SAX view, T2 mapping was carried out using the same geometrical parameters as T1 mapping and similar imaging parameters, including 340×340 mm^2 FOV, 1.5×1.5 mm^2 spatial resolution, 5∼6 slices, 5.0 mm slice thickness, 3.0 ms TR, 1.3 ms TE, 0/35/55 ms T2 preparation time, 6/8 partial Fourier, and R = 2 parallel imaging acceleration factor.

All the images were reconstructed using GeneRalized Autocalibrating Partially Parallel Acquisitions (GRAPPA). For the purpose of challenge, as shown in Fig. 1, we retrospectively undersampled the k-space data with acceleration factors of R = 4, 8, 10 with uniform sampling trajectory.

3.1.2. Annotation details

The myocardium and chambers were manually segmented by a skilled radiologist with over 5 years of expertise in cardiac imaging using ITK-SNAP (version 3.8.0). The original image coordinates were preserved in NIFTI format together with the segmentation labels and matching images. The labels we assigned to the segmented data contribute to improving the performance of certain reconstruction architectures. By incorporating this annotated information, the quality and accuracy of the reconstructed regions can be enhanced. The following four chamber labels apply to the LAX cine images:

(a) Label 1 for the left atrium;
(b) Label 2 for the right atrium;
(c) Label 3 for the left ventricle;
(d) Label 4 on the right ventricle.

We labeled the SAX cine images using the following definitions:

(a) Label 1 for the left ventricle blood pool;
(b) Label 2 for left ventricular myocardium;
(c) Label 3 for the right ventricle blood pool.

Both the T1 and T2 mapping annotations were identical to SAX cine.

3.2. Participants

The CMRxRecon Challenge is held in conjunction with the 26th International Conference on Medical Image Computing and Computer-Assisted Intervention (MICCAI 2023), on October 12th, 2023 in Vancouver, Canada. The official website for the CMRxRecon challenge is (https://cmrxrecon.github.io). As an open challenge, CMRxRecon received a total of 285 registration requests before the deadline preceding the MICCAI 2023 conference. Among them, 22 teams with 91 participants successfully submitted algorithm Docker containers for the testing phase before the submission deadline, as illustrated in Fig. 2. Among them, 7 teams submitted for both cine and mapping tasks. The 91 participants represent a diverse cohort hailing from 10 different countries. The details of all participating teams are summarized in Table 1. Note that a unique team index was assigned to each team participating in different tasks. For simplicity, we denote teams engaged in cine reconstruction as 'C*X*' and those involved in mapping reconstruction as 'M*X*'. We have carefully selected and extensively reported 10 representative algorithms, which included the results from the top 5 teams as well as the five teams that our organizers unanimously considered to be the most distinctive. The chosen algorithms take into account both novelty and performance evaluation. All teams have given their consent for the inclusion of their methods and results in this publication.

3.3. Challenge phases

The challenge includes three phases. First, to complete the registration and get access to the training and validation dataset, the participants were requested to register on the official challenge website, sign the data agreement, and keep their promise to abide by the challenge rules. Second, the participants were invited to take part in the validation phase, where the reconstructed images from under-sampled data are required to be submitted. The evaluation is automatically executed on the Synapse platform https://www.synapse.org/#!Synapse:syn51471091/wiki. The leaderboard is also presented online and updated promptly. Third, the participants were invited to take part in the final test phase to complete the full participation in this challenge. To guarantee the fairness of the competition, the packaged docker is the only valid submission in the test stage. Each team can submit 3 docker containers, and we will take the final submission as the official one. Our staff will run the docker container and confirm with the team that it has been successfully executed. Only completing the predictions of all test cases will be considered successful participation. The prizes are awarded to the top-3 teams of each task during the MICCAI conference. The top-3 teams in each task were invited to report their methodologies in the STACOM workshop on October 12, 2023.

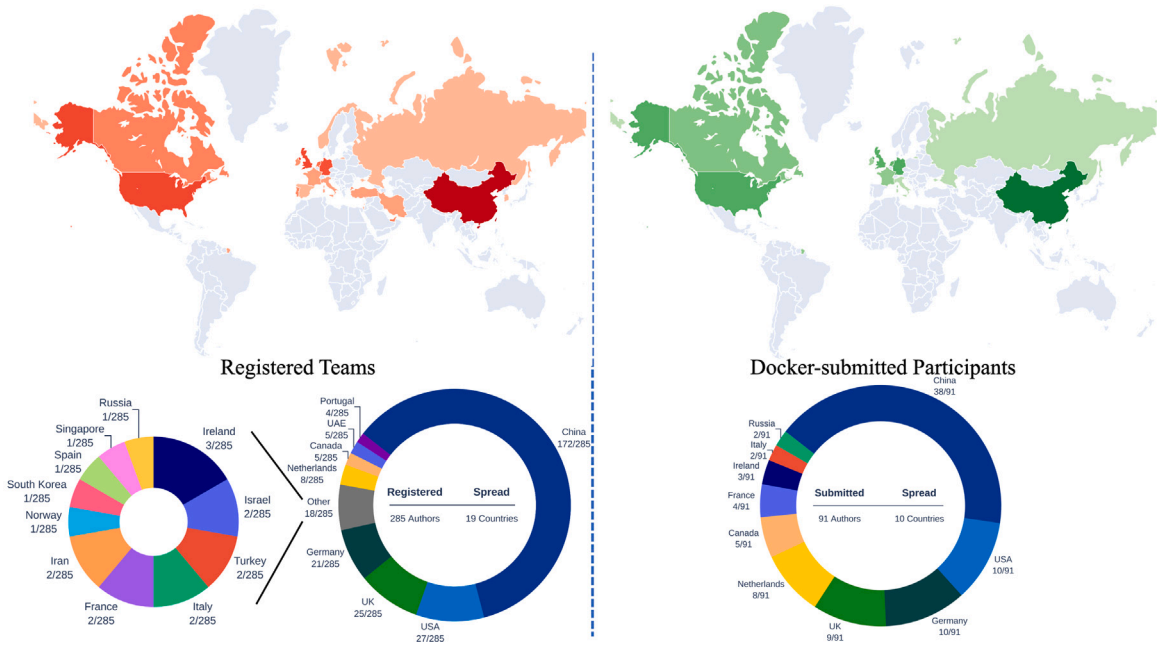

Fig. 2. The individual team statistics that registered and submitted the dockers for testing in the CMRxRecon Challenge.

Table 1
The list and details of the participants and teams who successfully participated in the test (docker-submission) phase.

Team name	Affiliation	Location
C1/M1. hellopipu	Department of Computer Science, Rutgers University	New Brunswick, USA
C2/M2. DIRECT	AI for Oncology, Netherlands Cancer Institute	Amsterdam, Netherlands
C3/M3. clair	Department of Imaging and Interventional Radiology, Faculty of Medicine, The Chinese University of Hong Kong	Hong Kong, China
C4. tjubiit	Tianjin Key Laboratory of Brain Inspired Intelligence Technology (BIIT), Tianjin University	Tianjin, China
M4. dbmapping	Department of Imaging Physics, Delft University of Technology	Delft, Netherlands
C5. imr	Canon Medical Systems (China) Co., Ltd.	Beijing, China
C6/M5. jabbers	Physikalisch-Technische Bundesanstalt (PTB)	Berlin, Germany
M6. whitealbum2	Nanjing University of Aeronautics and Astronautics	Nanjing, China
C7/M7. SkoICIG	Moscow, Skolkovo Institute of Science and Technology	Russia
C8. mataffine	School of Artificial Intelligence, Beijing Normal University	Beijing, China
M8/C11. Fast2501	Department of Biomedical Engineering, University of Virginia	Charlottesville, USA
C9. OREO	Beijing University of Posts and Telecommunications	Beijing, China
M9. imperial_cmr	National Heart and Lung Institute, Imperial College London	London, UK
C10. flyer	Department of Radiation Oncology, Peking University Cancer Hospital & Institute	Beijing, China
M10/C17. IADI-IMI	Institute of Medical Informatics, University of Lübeck; IADI, Inserm U1254	Lübeck, Germany; Nancy, France
C12. Edipo	School of Engineering, University of Edinburgh; Department of Information Engineering, University of Pisa	Edinburgh, UK; Pisa, Italy
C13. hkforest	Electronic and Computer Engineering, the Hong Kong University of Science and Technology	Hong Kong, China
M11. sunnybrook	Department of Medical Biophysics, University of Toronto	Toronto, Canada
C14. tsinghuacbir	Tsinghua University	Beijing, China
C15. insightdcu	Insight SFI Research Centre for Data Analytics, Dublin City University	Dublin, Ireland
C16. lyulab	Shenzhen Technology University	Shenzhen, China
C18. fzu312lab	Biomedical Engineering Institute of Fuzhou University	Fuzhou, China

3.4. Evaluation metrics

The reconstruction performance for both cine and mapping were assessed using the following criteria: peak signal-to-noise ratio (PSNR), normalized mean square error (NMSE), and structural similarity index measure (SSIM). For T1 and T2 mapping, we also calculated the quantitative T1 and T2 relaxation times in myocardium for comparison. The root mean square error (RMSE) for T1 and T2 values in myocardium was computed as evaluation metrics as well. We use the SSIM as our quantitative quality metric for ranking. For the cases without valid output, we will assign it to the lowest value of metric.

The metrics were defined as follows:

SSIM The SSIM index utilizes the inter-pixel relationships to assess the similarity between two images. The resemblance that results between two image patches, $\hat{m}$ and m, is described as follows.

$$\mathrm{SSIM}(\hat{m}, m) = \frac{\left(2\mu_{\hat{m}}\mu_m + c_1\right)\left(2\sigma_{\hat{m}m} + c_2\right)}{\left(\mu_{\hat{m}}^2 + \mu_m^2 + c_1\right)\left(\sigma_{\hat{m}}^2 + \sigma_m^2 + c_2\right)'} \tag{1}$$

where c_1 and c_2 are two variables to stabilize the division; $c_1 = \left(k_1 L\right)^2$ and $c_2 = \left(k_2 L\right)^2$. $\mu_{\hat{m}}$ and μ_m are the average pixel intensities in $\hat{m}$ and m, and their variances are $\sigma_{\hat{m}}^2$ and σ_m^2.

PSNR The power of the highest image intensity that may be achieved across a volume divided by the power of distortion-causing noise and

other defects is known as the PSNR.

$$\mathrm{PSNR}(\hat{v}, v) = 10\log_{10}\frac{\max(v)^2}{\mathrm{MSE}(\hat{v}, v)}. \quad (2)$$

Let v represent the target volume, $\hat{v}$ represent the reconstructed volume, $max(v)$ denote the largest entry in the target volume, and $\mathrm{MSE}(\hat{v}, v)$ be the mean square error between $\hat{v}$ and v, which is defined as $\frac{1}{n}||\hat{v} - v||_2^2$. Here, n represents the total number of entries in the target volume v.

NMSE The NMSE between a reference image or volume v and a reconstructed image or image volume expressed as a vector $\hat{v}$ is defined as:

$$\mathrm{NMSE}(\hat{v}, v) = \frac{\|\hat{v} - v\|_2^2}{\|v\|_2^2}, \quad (3)$$

where the squared Euclidean norm is represented by $\|\cdot\|_2^2$, and the subtraction is carried out entry-wise. We reported the NMSE values for the whole image volumes.

The Python scripts utilized for evaluating the image quality metrics can be found on GitHub at the following URL: https://github.com/CmrxRecon/CMRxRecon/tree/main/Evaluation.

4. Comparative overview on participants methodologies

This section provides a comprehensive comparison across various methodologies. A detailed summary of the 10 selected approaches is presented in . Within this table, we focus on delineating the principal contributions and the training strategies employed by the teams, providing a clear insight into the diverse techniques and their unique strengths. All participants trained their models from scratch on the CMRxRecon dataset.

Next, we report the methods from those selected teams in detail and highlight the key novelty or contribution of each method.

4.1. C1/M1 hellopipu

The team of *hellopipu* (C1/M1) proposed a two-stage MRI reconstruction pipeline to address the limitations of existing MRI reconstruction methods. Expanding on the foundation of E2E-VarNet (Sriram et al., 2020), the researchers introduced PromptMR (Xin et al., 2023), a comprehensive unrolled model for MRI reconstruction based on prompting. This model is versatile for handling diverse views, contrasts, adjacent types, and acceleration factors present in real clinical cardiac MRI scans. Within the architecture of PromptMR, each cascade integrates an image domain denoiser called PromptUnet, as shown in Fig. 3, and a k-space domain data consistency layer. PromptUnet employs a 3-level encoder–decoder architecture, featuring DownBlock, UpBlock, and PromptBlock at each level. The utilization of adjacent input (Fabian et al., 2022), which consists of a series of T1/T2 images or adjacent frames of the temporal cine, along with channel attention (Huang et al., 2019) in PromptUnet, facilitates the exploration of inter-frame and inter-contrast information. The PromptBlock, inspired by PromptIR (Potlapalli et al., 2023), encodes specific input-type context as an adaptively learned prompt across multiple levels to guide the reconstruction process. The multi-coil sensitivity maps are estimated by a compact PromptUnet from the central k-space which serves as the auto-calibration signal (ACS).

For training, both multi-coil SAX/LAX cine data and T1/T2-weighted data from the 120 healthy subjects in the dataset were employed. The input image to each PromptUnet in PromptMR was normalized using z-score normalization. Data augmentation during training focused on balancing the portion of SAX/LAX/T1/T2 slices. The complex image data was separated into 2 channels of real and imaginary parts as input to the network. A single PromptMR model with 12 cascades was trained. The model was optimized using the AdamW optimizer, configured with specific parameters: β_1 was set to 0.9, β_2 to 0.999, with a weight decay of 0.01. The training utilized SSIM loss across 12 epochs, starting with an initial learning rate of 10^{-4}, which was then reduced to 10^{-5} during the last epoch. Training took approximately 3 days on two NVIDIA A100 40 GB GPUs with a batch size of one per GPU. To refine the reconstruction results of PromptMR, two ShiftNet models (Li et al., 2023) and test time augmentation by flipping and 180-degree rotation were incorporated in the second stage. Each ShiftNet was trained with the initial cine or mapping reconstructions by PromptMR as the input. They used the Adam optimizer ($\beta_1 = 0.9$, $\beta_2 = 0.999$, and weight decay = 0), a batch size of one, cosine annealing learning rate schedule (base lr = 4×10^{-4}, $\eta_{min} = 1\times10^{-7}$), and SSIM loss to train ShiftNets for 50 epochs. The second stage of training took approximately 1 day for cine and 8 h for mapping on 8 A100 40 GB GPUs. The codebase for this approach is available at https://github.com/hellopipu/PromptMR.

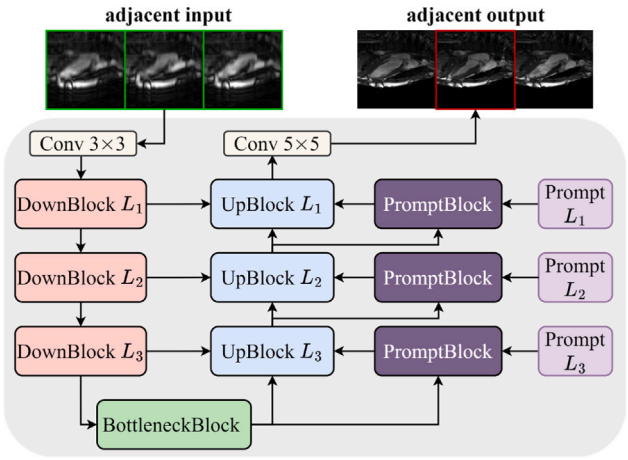

Fig. 3. Overview of PromptUnet proposed by the team *hellopipu* (C1/M1). PromptUnet serves as the denoiser in each cascade of PromptMR. It processes adjacent image frames to explore the inter-frame/-contrast information and incorporates a PromptBlock at each level to allow rich hierarchical context learning.

In summary, the design of PromptUnet plays a crucial role in leveraging adjacent k-space information and facilitating discriminative context learning for various MRI reconstruction tasks.

4.2. C2/M2 DIRECT

The team of *DIRECT* (C2/M2) formulated the reconstruction task as a least squares regularized optimization, with the adoption of vSHARP (Yiasemis et al., 2025), a variable Splitting Half-quadratic Alternating Direction Method of Multipliers (ADMM) algorithm (Fukushima, 1992) for the Reconstruction of Inverse-Problems, as the backbone. The team optimized the method for both 2D and 3D (2D + time/contrast) reconstructions, although their submitted model comprised the 3D vSHARP variant. This customized approach consists of three integral steps: first, a denoising step is implemented to refine the auxiliary variable; second, a data consistency step for the target image is executed through differentiable gradient descent over 8 iterations; and finally, an update mechanism for the Lagrange Multipliers is introduced by the ADMM. A distinctive feature of their approach is the integration of a Lagrange Multiplier Initializer, which utilizes a dilated convolution and replication padding module. This module, inspired by prior work (Yiasemis et al., 2022) and adapted for 3D applications, generates an initial estimate for the Lagrange Multipliers. The 2D dynamic vSHARP model took a sequence of 2D undersampled multi-coil k-space data (time-frames for cine tasks, contrast-frames for mapping tasks) as input and generated a corresponding sequence of 2D images as output for reconstruction. For each denoising step, distinct 3D U-Nets (Ronneberger et al., 2015) with four scales and 32 filters in the initial scale were employed. Due to the multi-coil nature of the data, a 2D U-Net (four scales, 32 channels in the first scale) was integrated for sensitivity map refinement from the ACS-k-space comprising 24 center lines (see Fig. 4).

Table 2
Summary of the strategies and contributions of the 10 selected teams.

Team name	Main novelty/contribution	Training strategy
C1/M1. hellopipu	•Use E2E-VarNet (Sriram et al., 2020) as backbone, introduce PromptMR, a prompting-based all-in-one unrolled model •Incorporate an image domain denoiser, PromptUnet, coupled with a k-space domain data consistency layer	•Data: multi-coil cine and mapping •Data separation: 120 cases for training. •Input: complex image data was separated into real and imaginary parts. A series of five T1/T2 images or adjacent frames of the temporal cine are used as input. •Learning Strategy: AdamW optimizer ($\beta1 = 0.9$, $\beta2 = 0.999$, weight decay = 0.01) over 12 epochs, with an initial learning rate of 1×10^{-4} and decayed to 1×10^{-5} in the last epoch •Normalization: z-score normalization •Loss: SSIM •Spatial–temporal Info: adjacent slices along contrast or temporal dimension were used for 2D slice reconstruction. •Code: https://github.com/hellopipu/PromptMR
C2/M2. DIRECT	•Use vSHARP (Yiasemis et al., 2025) as backbone, customize it to a 3D variant tailored specifically for 2D dynamic reconstruction; •Comprise three key steps: a denoising step to refine the auxiliary variable, a data consistency step for the target image performed through differentiable gradient descent over Tx=8 iterations, and an update for the Lagrange Multipliers introduced by ADMM	•Data: multi-coil cine and mapping •Data separation: 120 cases for training. •Input: complex data was separated into real and imaginary parts. •Learning Strategy: Adam optimizer ($\beta1 = 0.9$, $\beta2 = 0.999$, $\epsilon = 10^{-8}$), initial linear increase to 0.003 over 2k iterations, followed by a reduction every 50k iterations by a factor of 0.9 •Normalization: scaling the initial k-space with the 99.5% percentile value of its modulus •Loss: SSIM, SSIM3D, HFEN, and L1 losses in the image domain along with normalized mean absolute error (NMAE) and NSME losses in the k-space domain •Spatial–temporal Info: Two-dimensional dynamic reconstruction: 3D convolutions to handle 2D spatiotemporal (2D + time) data, exploiting temporal correlations. •Code: https://github.com/NKI-AI/direct
C3/M3. clair	•Use CAMP-Net (Zhang et al., 2023a) as backbone, propose k-t CLAIR (Zhang and Chen, 2023) incorporates self-consistency guidance and multiple priors in deep learning to exploit spatio temporal correlations across the x-t, x-f, and k-t domains	•Data: multi-coil cine and mapping •Data separation: 96 and 24 cases for training and validation. •Input: complex image data was separated into real and imaginary parts. •Learning Strategy: Adam optimizer ($\beta1 = 0.9$ and $\beta2 = 0.999$) 30/50 epochs with learning rate: 3×10^{-4} at initial and were reduced by a factor of 10 in the last 10 epochs. •Normalization: standard minmax of image volume per case. •Loss: SSIM and L1 •Spatial–temporal Info: 2D reconstruction. •Code: https://github.com/lpzhang/ktCLAIR
M4. dbmapping	•Use unrolling gradient descent scheme (Hammernik et al., 2018) as the backbone for multi-coil network •Introduce a relaxometry-informed quantitative MRI reconstruction method that synergizes joint mapping and unrolled gradient descent reconstruction,	•Data: multi-coil mapping •Data separation: 5-fold cross-validation with 96 cases for training and 24 cases for validation in each fold. •Input: the k-space data were segmented into real and imaginary parts. •Learning Strategy:Adam optimizer for 400 epochs with an initial learning rate 10^{-3} and a polynomial weight decay. •Normalization: min–max by the value at the 99th percentile of the frequency domain magnitude per slice. •Loss: L1, SSIM, and fitting loss in mapping •Spatio-temporal Info: k-space readouts at different relaxation times are cascaded along the channel direction and reconstructed simultaneously. •Code: https://github.com/pandafriedlich/relax_qmri_recon
C4. tjubiit	•Use soft data-consistency (Sriram et al., 2020) as the backbone and showcase a novel multi-scale inter-frame information fusion strategy. •Integrate distinct encoders dedicated to extracting features from each frame. These extracted features were then combined effectively using an information fusion block that incorporated multi-scale features from multiple frames.	•Data: multi-coil cine. •Data separation: 120, 60, and 120 cases for training, validation, and test. •Input: the real and imaginary components of the complex image data were concatenated along the channel dimension. •Learning Strategy: Adam optimizer with the initial learning rate 0.005 and scheduled to decay by a factor of 0.1 every 40 epochs. •Normalization: standardize z-score. •Loss: SSIM. •Spatial–temporal Info: 2D reconstruction. •Code: https://github.com/tjubiit-hub/CMR-recon
C7/M7. Skolcig	•Parameterize the objective function in compressed sensing (CS) minimization procedure by deep learning model (Kuzmina et al., 2022) as backbone. •Use meta-learning for CS minimization; for multi-coil, GRAPPA (Griswold et al., 2002) is first used initial estimation and used a simple U-net (Falk et al., 2019) to solve CS problem.	•Data: multi-coil and single-coil cine and mapping •Data separation: 120 training cases used for training. •Input: the k-space complex data. •Learning Strategy Adam optimizer ($\beta1 = 0.9$ and $\beta1 = 0.999$) and learning rate 10^{-3}. •Normalization: L2 normalization of k-space data for each 2D slice. •Loss: L1. •Spatial–temporal Info: 2D reconstruction. •Code: https://github.com/Airplaneless/cmrx

(*continued on next page*)

Table 2 (*continued*).

Team name	Main novelty/contribution	Training strategy
M8. Fast2501	•Use a 2D U-Net (Ronneberger et al., 2015) as the backbone network structure and propose a complex-valued cascading cross-domain convolutional neural network. •Alternate between the restoration step and the data consistency step.	•Data: multi-coil cine and mapping. •Data separation: 90, 10 and 20 cases for training, validation, and testing. •Input: complex data was directly used since the network is fully complex-valued. •Learning: Adam optimizer for 50 epochs with a learning rate of 0.0001, $\beta 1 = 0.9$, $\beta 2 = 0.999$, and $\epsilon = 10^{-8}$. •Normalization: k-space data for each 2D slice was scaled to have its magnitude between 0 to 1. •Loss: L1 and SSIM. •Spatial–temporal info: 2D reconstruction. •Code: https://github.com/qd9zb/CMRxRecon
C12. Edipo	•Use convolutional recurrent neural network(CRNN) (Qin et al., 2018) and single-image super-resolution network, Bicubic++ (Bilecen and Ayazoglu, 2023), as the backbone. •Propose an additional bidirectional convolutional recurrent unit (BCRNN) followed by a lightweight refinement module.	•Data: single-coil cine. •Data separation: 90, 20, and 10 cases for training, validation, and testing. •Input: complex image data was separated into magnitude and phase parts. •Learning Strategy: Adam optimizer($\beta 1 = 0.9$, $\beta 1 = 0.999$, weight decay 0.0) for 50 epochs with the initial learning rate 3×10^{-4} gradually reduced to 3×10^{-6} with the StepLR scheduler •Normalization: minimax using 1% or 99% percentile per subject •Loss: L1 and SSIM. •Spatial–temporal Info: 2D reconstruction. •Code: https://github.com/vios-s/CMRxRECON_Challenge_EDIPO
C15. insightdcu	•Use Unet (Falk et al., 2019) as the backbone, enhanced by Group Normalization (GN) and channel attention layers (Gated Channel Transformation: GCT) (Yang et al., 2020).	•Data: single-coil cine. •Data separation: random sampling strategy to obtain 1000 LAX and 1000 SAX image slices for training. •Input: complex image data was separated into real and imaginary parts. •Learning Strategy: AdamW optimizer with a learning rate of 0.001. •Normalization: scaled by the maximum signal intensity and further min–max scaled into the range of [0, 1]. •Loss: MSE. •Code: https://github.com/juliadietlmeier/CMRxRecon_insightdcu
C17. IADI-IMI	•Use multi-resolution hash encoding (Müller et al., 2022) and JSENSE (Ying and Sheng, 2007) for implicit sensitivity map estimation as backbone. •Consist of two shallow MLP networks for the simultaneous prediction of a complex-valued intensity reconstruction and a set of complex-valued coil sensitivity maps.	•Data: multi-coil cine. •Data separation: 0 for training (instance-optimization) and 20 for testing. •Input: complex image data as imaginary and real parts, combined input of adjacent temporal frames. •Learning strategy: Adam optimizer ($\beta_1 = 0.9$, $\beta_2 = 0.99$) with a learning rate of 10^{-2} for 200 iterations. •Normalization: each under-sampled multi-coil 2D+t k-space was scaled by the maximum intensity of its SOS magnitude reconstruction. •Loss: Huber loss ($\delta = 1.0$) and total-variation regularization. •Spatial–temporal Info: 2D+t Hash encodings ensure spatio-temporal consistency. •Code: https://github.com/MDL-UzL/CineJENSE

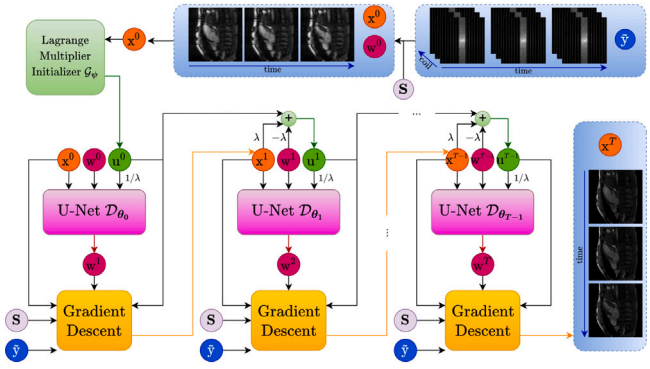

Fig. 4. Overall workflow of the proposed vSHARP by team *DIRECT*(C2/M2).

The original complex data was separated into a 2-channel format as input to the network. To ensure robust training, normalization involved scaling the initial k-space with the 99.5% percentile value of its modulus. Model performance was enhanced through techniques such as joint modality training (cine and mapping data concurrently) and augmentations like k-space flipping, random k-space cropping, and multi-scheme undersampling (radial, spiral, variable density, random and equispaced rectilinear following methods presented in (Yiasemis et al., 2024)). Additionally, the model simultaneously underwent training for all acceleration factors (4, 8, and 10). A dual-domain loss function was employed, encompassing SSIM, SSIM3D, HFEN, and L1 losses in the image domain, along with NMAE and NSME losses in the k-space domain. The end-to-end pipeline underwent training for approximately 1 million iterations (around 25 days) using the Adam optimizer ($\beta 1 = 0.9$, $\beta 2 = 0.999$, $\epsilon = 10^{-8}$) for parameter optimization. The learning rate underwent an initial linear increase to 0.003 over 2k iterations, followed by a reduction every 50k iterations by a factor of 0.9. Training was conducted on four NVIDIA A100 80 GB GPUs, with a batch size of 1 on each GPU. They trained their proposed method on all provided training data and evaluated it on the validation set using the tool provided by the challenge. The time required for the reconstruction of a single 4D (space dimensions + time/contrast) volume varied between 2.7 to 15.7 s. The code for this training strategy is openly accessible at https://doi.org/10.21105/joss.04278.

In summary, the novel aspect lies in its integration of a Lagrange Multiplier Initializer combined with advanced denoising and data consistency mechanisms within a variable splitting ADMM framework, optimized for both 2D and 3D quantitative MRI reconstructions.

4.3. C3/M3 clair

The team *clair*(C3/M3) introduced k-t CLAIR which adopted the unrolled-based CAMP-Net (Zhang et al., 2023a) as the foundational

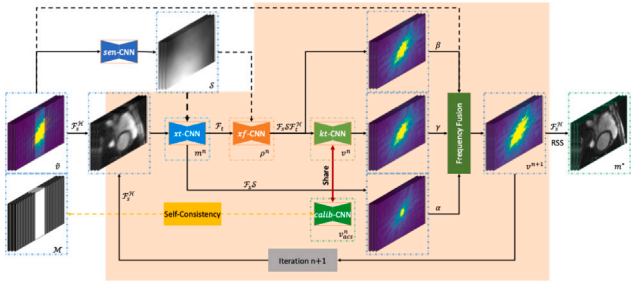

Fig. 5. The proposed k-t CLAIR by team *clair*(C3/M3) exploits spatiotemporal correlations in data and incorporates calibration information to learn complementary priors across the x-t, x-f, and k-t domains.

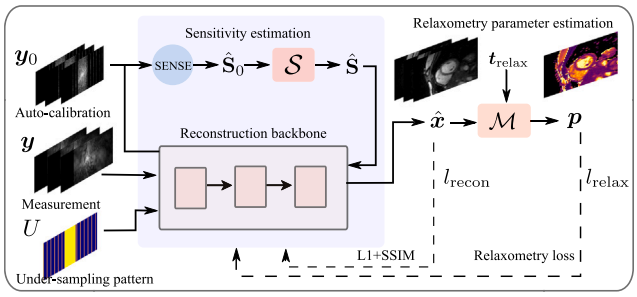

Fig. 6. The relaxometry-informed quantitative MRI reconstruction method that synergizes joint mapping and unrolled gradient descent reconstruction developed by the team *dbmapping*(M4).

framework and expanded its capabilities to address dynamic and parametric CMR, as described in Fig. 5. By exploiting spatiotemporal correlations, k-t CLAIR learns complementary priors in the x-t, x-f, and k-t domains, while enforcing self-consistency learning in the k-t domain. The approach involves four key steps within each iteration: image enhancement in the x-t domain using xt-CNN, dynamic temporal prior learning in the x-f domain through xf-CNN, k-space restoration in the k-t domain using kt-CNN, and self-consistency learning in the k-t domain via calib-CNN. During each iteration, the approach outlines the reconstruction steps in the x-t, x-f, and k-t domains, leveraging spatiotemporal correlations and periodic cardiac motion for effective dynamic feature restoration. A frequency fusion block is introduced to coordinate feature learning processes, and joint learning of coil sensitivity maps with sen-CNN enhances the reconstruction process. Calibration information is integrated into the k-t domain to ensure accurate signal restoration. U-Net is utilized for highly nonlinear prior learning, and a frequency fusion layer balances contributions from different priors. The frequency fusion block facilitates the coordination of different priors, contributing to accurate and faithful dynamic MRI reconstruction.

Distinct models were trained for multi-coil cine and T1/T2 mapping data. The training utilized 80% of the 120 healthy subjects, while the remaining 20% were reserved for model validation. An additional 60 healthy subjects were included for online testing, and no data processing or augmentation, except for data standardization, was applied. The original complex data was separated into two channels: phase and magnitude, serving as inputs to the networks. Model optimization employed the Adam optimizer ($\beta 1 = 0.9$ and $\beta 2 = 0.999$) along with SSIM and L1 losses for 30/50 epochs for the Cine/Mapping task, initiating with a learning rate of 3×10^{-4} and a batch size of 1. Learning rates were reduced by a factor of 10 in the last 10 epochs. The number of iterations was set to 12 for all rolling-based models. The GitHub repository is accessible at: https://github.com/lpzhang/ktCLAIR

In summary, the team introduces a novel approach that leverages multi-domain learning and spatio-temporal correlations in dynamic and parametric CMR, integrating a frequency fusion block and self-consistency learning for enhanced dynamic MRI reconstruction.

4.4. M4 dbmapping

The team *dbmapping* (M4) proposes a relaxometry-guided reconstruction pipeline for the quantitative mapping subtask. The design of the reconstruction backbone follows the unrolling gradient descent scheme (Hammernik et al., 2018). In each layer, data fidelity is constrained in the frequency domain, and a U-Net is dedicated to learning the image prior in a data-driven fashion. They exclusively used multi-coil acquisitions for reconstruction. Following Yiasemis et al. (2022), the coil sensitivity map was initially estimated by the SENSE (Pruessmann et al., 1999) operator and then refined by a learnable U-Net. Compared to traditional reconstruction, quantitative MRI reconstruction differs from other types of MRI in the sense that the reconstructed images should conform to the relaxometry. Taking advantage of this additional relaxometry prior, they proposed a joint mapping and reconstruction framework and employed an unsupervised mapping network to estimate the relaxometry-related parameters like T1 and T2 (see Fig. 6).

Multi-coil acquisitions were treated as image channels in the 2D reconstruction pipeline, and all baseline images were reconstructed simultaneously. The T1- and T2-mapping networks were trained to minimize the fitting loss induced by the relaxometry and estimate the quantitative parameters. Afterward, the mapping networks were frozen and incorporated into the reconstruction pipeline as relaxometry guidance. They trained separate neural networks for each acceleration factor (4/8/10) and each imaging sequence (MOLLI/T2-prep). The networks were trained in a 5-fold cross-validation manner using the Adam optimizer for 400 epochs, with an initial learning rate of 1×10^{-3} and polynomial weight decay. A combination of L1, SSIM, and the fitting loss in the mapping was used as the training loss. At inference time, an ensemble of the 5 models was used for the final prediction. The GitHub repository is accessible at: https://github.com/pandafriedlich/relax_qmri_recon

In summary, the joint mapping and reconstruction framework allows direct quantitative parameter estimation and improves the reconstruction quality.

4.5. C4 tjubiit

The team *tjubiit*(C4) presents an advanced approach to dynamic parallel MRI reconstruction, emphasizing a novel multi-scale inter-frame information fusion strategy, as shown in Fig. 7. The method is designed to extract and leverage multi-scale features from adjacent multi-frame data, enhancing the overall reconstruction process. Specific encoders are employed for feature extraction from each frame, contributing to a nuanced understanding of information at different scales. The introduced information fusion block effectively combines these multi-scale features from multiple frames, enabling the comprehensive utilization of supplementary information. Additionally, the fused inter-frame information plays a crucial role in subsequent refinement blocks, guiding feature enhancement and contributing to the overall reconstruction quality. The proposed framework strategically incorporates several specific encoders for feature extraction from each frame in the inter-frame information fusion stage. This ensures a nuanced understanding of information at different scales, allowing for effective utilization of supplementary information from multiple frames. The information fusion block effectively combines the multi-scale features of multiple frames, facilitating comprehensive information utilization. Moreover, the fused inter-frame information is utilized in subsequent refinement blocks to enhance feature and guide the reconstruction process. In the refinement stage, the method introduces an Inter-Frame Features Enhancement (IFFE) Net, which focuses on utilizing reference

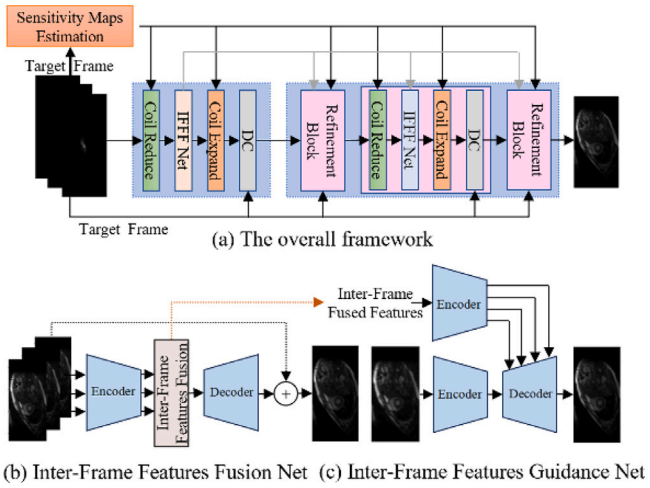

Fig. 7. The implementation of proposed Multi-Scale Inter-Frame Information Fusion Based Network by team *tjubiit*(C4).

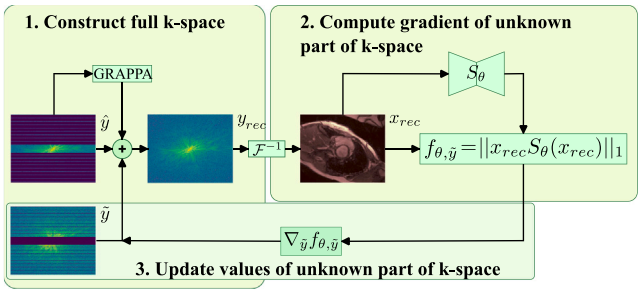

Fig. 8. Inference of the method of utilizing U-net like CNN for compressed sensing reconstruction developed by team *Skolcig*(C7/M7). In the case of multi-coil data, $y_{rec} = \hat{y} + \tilde{y} + y_{grappa}$ where y_{grappa} is the prediction of missing k-space data by GRAPPA convolution.

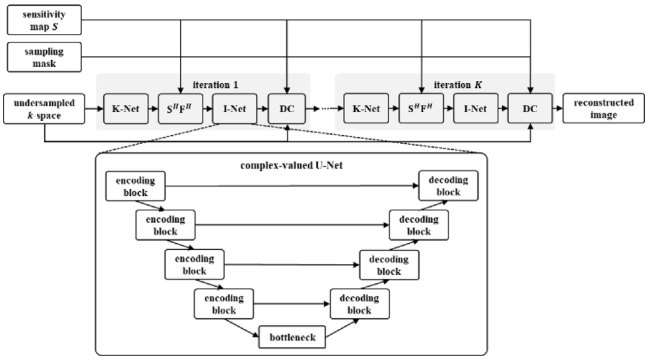

Fig. 9. The C^3-Net present by team *Fast2501*(M8) alternates between the restoration step and the data consistency step. Both the k-space subnetwork and the image subnetwork use a complex-valued U-Net.

frame features for further enhancement. The IFFE Net adopts a U-Net architecture and introduces an Inter-Frame Features Enhancement Block (IFFEB) with spatial and channel attention mechanisms. Enhanced features are derived from a combination of spatial and channel attention maps, contributing to overall improvements in dynamic MRI reconstruction.

The multi-coil cine k-space data, derived from the 120 subjects underwent division into 40% for training, 20% for validation, and 40% for testing. The team employed two distinct data augmentation techniques. Specifically, spatial domain data underwent random vertical and horizontal flipping, as well as rotation at an angle not exceeding 45°, each with a defined probability. The real and imaginary components of the data were concatenated along the channel dimension and input into multiple cascaded networks. Different channels shared the same encoder–decoder network for estimating sensitivity maps from low-frequency data images. The framework ultimately integrated a soft data consistency layer (Sriram et al., 2020) to enhance fidelity. Following this, the frequency domain output underwent sequential processing involving inverse Fourier transform, absolute value calculation, and root sum squares calculation. Subsequently, supervised training was conducted using the SSIM loss. The initial learning rate for training was set to 0.005 and scheduled to decay by a factor of 0.1 every 40 epochs. The GitHub repository is accessible at: https://github.com/tjubiit-hub/CMR-recon

In summary, the introduced multi-scale inter-frame information fusion strategy not only significantly enhanced the overall reconstruction performance but also demonstrated a high level of efficiency.

4.6. C7/M7 Skolcig

The team *Skolcig*(C7/M7) utilizes a novel approach by parameterizing the objective function in the compressed sensing (CS) minimization procedure through a deep learning model, specifically employing the model proposed in Autofocusing+ (Kuzmina et al., 2022) as a backbone. This can be regarded as meta-learning for CS minimization, as described in Fig. 8. A commonly used objective function for compressed sensing is the L1-norm of the reconstructed image, denoted as $\|x_{rec}\|_1$. The SkolCIG team extended this function to $\|x_{rec} S_{\theta,i}(x_{rec})\|_1$, where $x_{rec}(\tilde{y}) = \text{rss}(\mathcal{F}^{-1}(\hat{y} + \tilde{y}))$ represents the estimation of the reconstructed image for a given sampled k-space $\hat{y}$, and $\tilde{y}$ is an estimate of unknown k-space data. $S_{\theta,i}(\cdot)$ denotes a U-net model with θ parameters on the ith optimization step.

In the case of multi-coil k-space data, the estimation of the reconstructed image is given by $x_{rec}(\tilde{y}) = \text{rss}(\mathcal{F}^{-1}(\hat{y} + y_{grappa} + \tilde{y}))$, where y_{grappa} is the estimation of the unknown part of the k-space using the GRAPPA method (Griswold et al., 2002). The central 24 lines of k-space data were utilized for GRAPPA kernel estimation. The CS minimization $\tilde{y} = \arg\min \|x_{rec} S_{\theta,i}(x_{rec})\|_1$ was performed using Adam optimization. The parameters of the U-net θ were also optimized by Adam optimization with parameters $\beta_1 = 0.9$, $\beta_2 = 0.999$, and a learning rate of 10^{-3}. The SkolCIG team employed a simple U-net model (Ronneberger et al., 2015) with 32 channels and 4 pool layers, incorporating instance norm and SiLU activation. Training such a U-net requires second-order gradients and storing the entire computational graph for CS optimization, making it a computationally and memory-intensive task. Therefore, they were constrained to 5 Adam optimization steps for $\tilde{y} = \arg\min \|x_{rec} S_{\theta,i}(x_{rec})\|_1$ minimization. The implementation of this approach is available at https://github.com/Airplaneless/cmrx.

In summary, they introduce a meta-learning framework for compressed sensing by parameterizing the L1-norm objective function with a U-net model, optimizing both the reconstructed image and U-net parameters through iterative minimization.

4.7. M8 Fast2501

The team *Fast2501*(M8) presents a sophisticated approach named C^3-Net—a complex-valued cascading cross-domain convolutional neural network designed for the reconstruction of undersampled CMR images, as shown in Fig. 9. The C^3-Net alternates between restoration and DC steps, incorporating a k-space subnetwork and an image subnetwork. Both subnetworks leverage a 2D U-Net (Ronneberger et al., 2015) as the backbone structure, featuring a sequence of complex-valued encoding or decoding blocks.

Separate models were trained for the cine and mapping tasks. The 120 fully sampled multi-coil subjects were randomly divided into 90 for training, 10 for validation, and 20 for testing. The magnitude

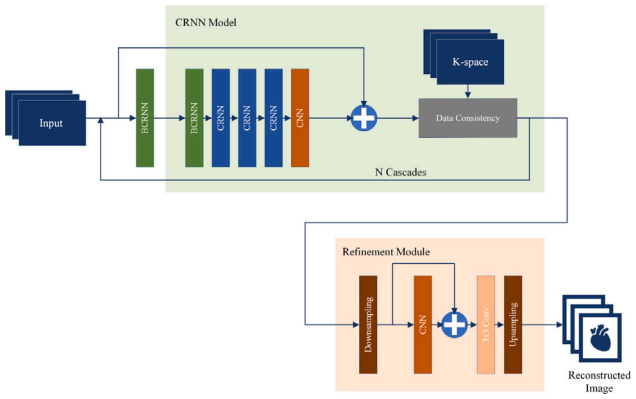

Fig. 10. The proposed model architecture by team *Edipo*(C12): BCRNN, CRNN, and CNN units with a data consistency (DC) step for primary reconstruction. The low-cost refinement module includes downsampling (DS), CNN, and upsampling (US) units.

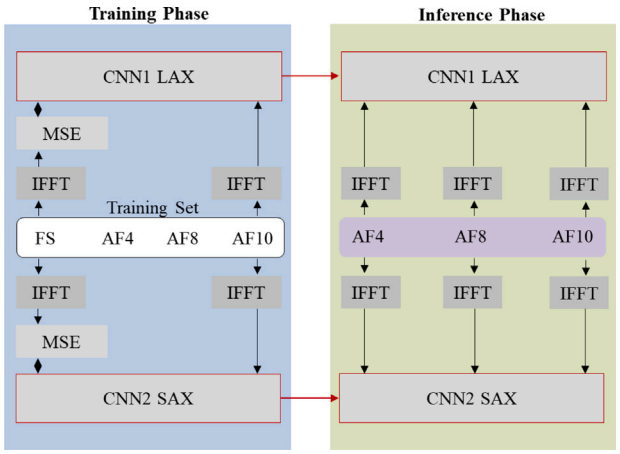

Fig. 11. Architecture of the proposed double-stream cardiac MRI reconstruction pipeline by team *insightdcu*(C15). Double-stream IFFT and CNN pipeline processes LAX and SAX images separately. The denoising CNN1 and CNN2 are two identical UNET-based models (GNA-UNET). AF4, AF8, and AF10 are abbreviations for acceleration factors 4, 8, and 10, respectively.

of k-space data for each 2D slice was scaled to range from 0 to 1. Training augmentation included random flipping along readout and phase encoding directions. During training, the undersampling ratio was randomly chosen between 4 to 12, and the equispaced undersampling mask was generated dynamically. The central 24-phase encoding lines were consistently fully sampled, and sensitivity maps were precomputed from the time-averaged autocalibration signal region using ESPIRiT (Uecker et al., 2014). All subnetworks in the reconstruction pipeline underwent joint end-to-end training, utilizing a mixed L1 and SSIM loss. The training was conducted with an Adam optimizer for 50 epochs, employing a learning rate of 0.0001, $\beta 1 = 0.9$, $\beta 2 = 0.999$, $\epsilon = 10^{-8}$. The GitHub repository is accessible at: https://github.com/qd9zb/CMRxRecon

In summary, the proposed C^3-Net effectively integrates the complex value of MR data and coupled information from both the k-space domain and image domain within the model. This integration results in a substantial improvement in image quality, particularly at high acceleration rates.

4.8. C12 Edipo

The team *Edipo*(C12) investigate the use of a convolutional recurrent neural network (CRNN) (Qin et al., 2018) architecture and the single-image super-resolution network, Bicubic++ (Bilecen and Ayazoglu, 2023) to exploit temporal correlations in supervised cine cardiac MRI reconstruction. In their proposed end-to-end network, as shown in Fig. 10, they introduced an additional bidirectional convolutional recurrent unit (BCRNN) onto CRNN to specifically address motion artifacts by further exploiting spatio-temporal correlations. Following the CRNN module, a DC module was incorporated to enforce alignment between the reconstructed k-space and the lines acquired from the undersampled data. Lastly, a lightweight refinement module, inspired by super-resolution networks, was extended to enhance image details while maintaining a short reconstruction time. This comprehensive framework effectively leverages spatio-temporal correlation to tackle motion artifacts and aliasing artifacts, resulting in improved image details while ensuring computational efficiency.

During the training process, only single-coil raw k-space data was utilized. The provided training dataset included ground truth reference data from 120 subjects, which the Edipo team split in a 90 : 20 : 10 ratio for training, evaluation, and testing, respectively. To enhance the model's robustness, they jointly trained the SAX and LAX data during the training phase. The raw complex data were split into phase and magnitude channels, serving as inputs to both the CRNN module and the DC module. For detail refinement in the reconstruction, the intermediate two-channel results were merged into single-channel magnitude data, which was then fed into the refinement module to obtain the final reconstructed image. Training the model employed the Adam optimizer ($\beta 1 = 0.9$, $\beta 2 = 0.999$, weight decay = 0) and L1 loss, along with SSIM loss, for 50 epochs. The initial learning rate started at 3×10^{-4} and gradually reduced to 3×10^{-6} with the StepLR scheduler. The GitHub repository for their work is accessible at https://github.com/vios-s/CMRxRECON_Challenge_EDIPO.

In summary, integrating a bidirectional CRNN with a DC module and a super-resolution-inspired refinement module can effectively address motion artifacts and improve image detail with computational efficiency.

4.9. C15 insightdcu

The team *insightdcu*(C15) devised a double-stream pipeline to process LAX and SAX data streams independently, as demonstrated in Fig. 11. Notably, they focused their denoising CNN training exclusively on ×10 undersampled images (AccF10), which exhibit the most prominent aliasing artifacts. Their denoising pipeline employed a UNET-based backbone named GNA-UNET, enriched with Group Normalization (GN) and channel Attention layers on the image domain. This GNA-UNET model adheres to the classical UNET architecture (Ronneberger et al., 2015), featuring five encoder–decoder blocks and initiating with 64 feature maps in the initial encoder block. Dropout layers were strategically added for regularization. The authors conducted an Ablation Study, revealing that the inclusion of GN layers led to an approximate 2 dB PSNR gain when evaluated on a subset of the training set. Additionally, the incorporation of channel attention (Gated Channel Transformation: GCT) (Yang et al., 2020) layers resulted in a performance gain, albeit of a lower magnitude (0.02 dB). The encoder block in the GNA-UNET model comprises conv_block(in_channels, out_channels)→Dropout(p = 0.25)→MaxPooling2d(2,2) layers. The conv_block includes conv2d(kernel_size=3, padding=1)→GCT→GN(ng)→conv2d (kernel_size=3, padding=1)→GCT→GN(ng)→ReLU. Here, GN(ng) represents a group normalization layer with the hyperparameter ng = 8, determined in the Ablation study. The decoder block mirrors the encoder block in reverse and involves a combination of the transposed convolution layer ConvTranspose2d (kernel_size=2, stride=2, padding=0)→conv_block. The total number of learnable parameters in the GNA-UNET is 124,427,137.

To facilitate rapid experimentation, the team employed a random sampling strategy, selecting 1000 LAX and 1000 SAX images for training from the whole dataset. The loss function utilized was MSE, and

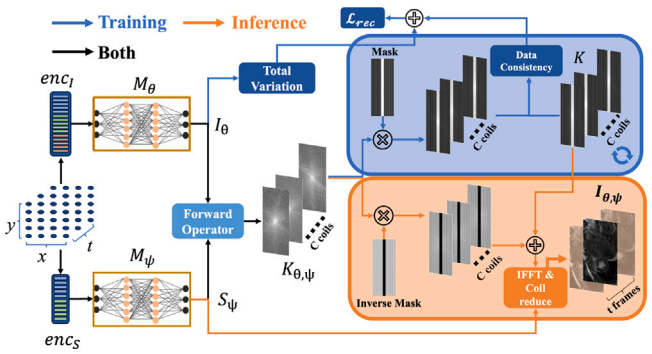

Fig. 12. The CineJENSE model proposed by the team of *IADI-IMI*(C17) consists of two MLP networks, M_θ and M_ψ, that receive hash grid encoded 2D+t coordinates as input and predict complex image reconstructions and sensitivity maps, respectively. The forward operator yields coil-expanded k-space predictions that are considered for masked data consistency optimization at training time. At inference time, the inverse mask is used to fill the missing lines of the acquired k-space data, and the final reconstruction is obtained by coil reduction using the estimated sensitivity maps.

AdamW served as the optimizer with a learning rate of 0.001. The model underwent training for 300 epochs to ensure convergence, with no data augmentation applied during this phase. The batch size was set to 2, and the images were resized to a 512 × 512 input resolution. The images were normalized using a min–max method to the range of [0, 1].

In summary, the pivotal addition of Group Normalization layers in the GNA-UNET model yielded the most substantial performance gain.

4.10. C17 IADI-IMI

The team *IADI-IMI*(C17) employs an Implicit Neural Representation (INR) backbone with multiresolution hash encoding (Müller et al., 2022) for the task of multi-coil cine reconstruction. Their developed instance optimization method CineJENSE (Al-Haj Hemidi et al., 2023), depicted in Fig. 12, draws inspiration from the physics model JSENSE (Ying and Sheng, 2007) and is an adaptation of IMJENSE (Feng et al., 2023), tailored for dynamic MRI and implicit sensitivity map estimation.

The proposed model comprises two shallow MLP networks that simultaneously predict a complex-valued intensity reconstruction and a set of complex-valued coil sensitivity maps. A multiresolution hash grid encodes spatial–temporal information, mapping 2D+t input coordinates to a higher-dimensional encoding optimized for the task. The multiplication of outputs from both MLP networks results in coil-expanded reconstructions, subsequently transformed into multi-coil k-space predictions through Fourier transformation. During training, predictions are masked with the acquisition mask for DC evaluation, while at inference time, predicted k-space lines of the inverse mask are considered to fill the missing lines of the acquired data. Following an unsupervised instance optimization approach, the model underwent validation on 20 healthy subjects from the training dataset, covering both SAX and LAX cine for all acceleration factors. The proposed 2D+t model processed slices independently following the physics model of JSENSE (Ying and Sheng, 2007) while leveraging the temporal information of all cardiac phases. Each undersampled multi-coil 2D+t k-space was scaled by the maximum intensity of its sum-of-squared magnitude reconstruction. The model was trained for 200 iterations using an Adam optimizer ($\beta 1 = 0.9$, $\beta 2 = 0.99$) with a learning rate of 1×10^{-2}. To ensure k-space fidelity and denoised intensity reconstructions, the model applied Huber loss ($\delta = 1.0$) and total variation regularization, respectively. The GitHub repository for their work is accessible at https://github.com/MDL-UzL/CineJENSE.

In summary, CineJENSE presents a lightweight solution for simultaneous coil sensitivity estimation and cine reconstruction, harnessing spatiotemporal correlations to derive accurate reconstructions from under-sampled k-space acquisitions without requiring fully-sampled reference training data.

Table 3
Evaluation results on cine of CMRxRecon challenge achieved by participants. The results are reported in the format of mean ±standard deviation.

Rank	TeamName	SSIM	PSNR	NMSE
1	hellopipu	0.990 ± 0.002	46.873 ± 1.424	0.003 ± 0.001
2	Direct	0.988 ± 0.003	46.161 ± 1.381	0.004 ± 0.001
3	clair	0.986 ± 0.003	45.221 ± 1.536	0.005 ± 0.002
4	tjubiit	0.984 ± 0.003	43.791 ± 1.401	0.007 ± 0.002
5	imr	0.983 ± 0.003	43.635 ± 1.456	0.007 ± 0.002
6	Jabber	0.981 ± 0.008	35.777 ± 1.308	0.048 ± 0.017
7	SkoICIG	0.969 ± 0.006	41.133 ± 1.556	0.030 ± 0.006
8	Mataffine	0.967 ± 0.006	39.905 ± 1.371	0.014 ± 0.004
9	OREO	0.958 ± 0.007	37.730 ± 1.371	0.024 ± 0.009
10	feiwang	0.957 ± 0.024	39.196 ± 1.439	0.019 ± 0.007
11	Fast2501	0.951 ± 0.015	36.443 ± 1.905	0.077 ± 0.036
12	Edipo	0.946 ± 0.009	35.582 ± 1.313	0.037 ± 0.012
13	hkforest	0.945 ± 0.008	35.777 ± 1.309	0.048 ± 0.017
14	tsinghuacbir	0.923 ± 0.012	36.660 ± 1.361	0.030 ± 0.010
15	insightdcu	0.921 ± 0.015	34.449 ± 1.455	0.056 ± 0.022
16	Lyu lab	0.913 ± 0.019	32.812 ± 1.847	0.093 ± 0.051
17	IADI-IMI	0.911 ± 0.015	39.048 ± 1.822	0.025 ± 0.016
18	Fzu312lab	0.793 ± 0.098	25.387 ± 2.458	0.588 ± 0.344

5. Statistical analysis and summary of challenge outcomes

5.1. Overall outcome

The challenge has attracted over 285 teams with more than 600 participants. These participants come from 19 countries and regions worldwide. Our official website has received over 15,000 visits, with more than 1100 users from 38 countries. We have evaluated over 1000 submissions during the validation phase (642 submissions for Task 1, and 362 submissions for Task 2), and more than 500 of them have received valid scores on the leaderboard and detailed log files. During the testing phase, we received over 90 Docker images from 22 teams. All the Dockers were successfully run by the organizers.

5.2. Quantitative and qualitative comparisons

Table 3 and Table 4 respectively reported the quantitative evaluation results of cine and mapping reconstruction from different participated teams. Fig. 13, 14 , 17, 18 show the visualization of the top 5 teams of the two tasks (see Figs. 15 and 16).

The evaluation criteria used in this challenge include PSNR, SSIM, and NMSE. For the final rankings, we considered the higher SSIM value between the multi-coil and single-channel reconstruction results as the final score for ranking. The mean SSIM of images reconstructed from different undersampling rates (R4, R8 and R10) were chosen as the ranking criteria respectively. Quantitative results indicate that the team "hellopipu" achieved outstanding performance across all metrics. A further RMSE on mapping was evaluated between the myocardium part of the ground truth and reconstructed images.

For the mapping task, a better SSIM on the original images does not necessarily guarantee improved measurements of the mapping values. For example, "clair" reached the second lowest RMSE among all the teams but got third place according to both NMSE and SSIM in the mapping task in Table 4.

5.3. Consensus on effective strategies

Tables 7 and 8 respectively outline the key characteristics of the 18 models for cine reconstruction and 11 models for mapping reconstruction. Although we did not specifically encourage teams to perform multi-coil reconstruction, it is worth noting that the majority of

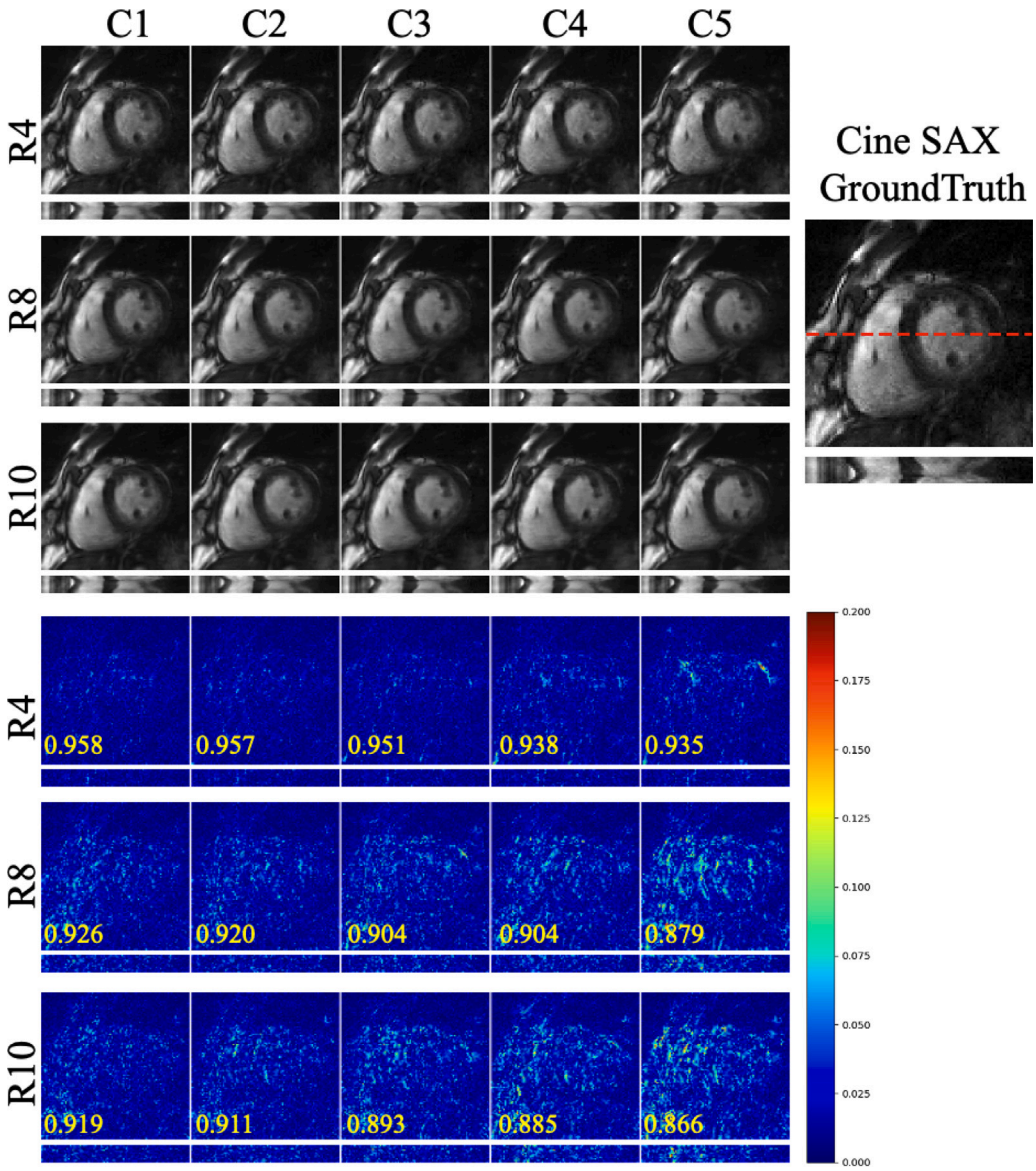

Fig. 13. Performances of the top 5 teams in cine task with SAX view under acceleration factors of 4, 8, and 10. The SSIM of each team is listed in the bottom left corner.

Table 4
Evaluation results on mapping of CMRxRecon challenge achieved by participants. The results are reported in the format of mean ±standard deviation.

Rank	TeamName	SSIM	PSNR	NMSE	Mapping RMSE
1	hellopipu	0.987 ± 0.007	45.481 ± 2.705	0.004 ± 0.002	24.10 ± 1.554
2	Direct	0.984 ± 0.008	44.346 ± 2.600	0.004 ± 0.002	26.03 ± 1.312
3 (tie)	clair	0.983 ± 0.008	43.937 ± 2.527	0.005 ± 0.003	24.61 ± 1.554
3 (tie)	dbmapping	0.983 ± 0.008	44.004 ± 2.680	0.005 ± 0.003	27.35 ± 1.671
4	Jabber	0.977 ± 0.009	41.590 ± 2.333	0.008 ± 0.003	37.00 ± 2.694
5	whitealbum2	0.958 ± 0.012	38.176 ± 2.401	0.033 ± 0.008	56.32 ± 7.762
6	SkoICIG	0.963 ± 0.012	39.403 ± 2.436	0.030 ± 0.010	55.48 ± 8.514
7	Fast2501	0.934 ± 0.021	33.087 ± 2.255	0.069 ± 0.032	69.10 ± 10.81
8	imperial_cmr	0.899 ± 0.025	35.628 ± 2.329	0.065 ± 0.031	66.66 ± 3.293
9	IADI-IMI	0.812 ± 0.067	36.796 ± 2.512	0.026 ± 0.013	47.39 ± 4.758
10	sunnybrook	0.771 ± 0.085	33.690 ± 2.399	0.047 ± 0.025	60.16 ± 8.104

participating teams chose to use multi-coil data for reconstruction. The teams demonstrated improved performance when utilizing multi-coil reconstruction compared to single-coil approaches, which is within our expectations. In this section, we provide the summary of several effective strategies to cope with CMRxRecon. These characteristics include the backbone architecture, data standardization, data augmentation strategies, and whether a physical model is employed.

5.3.1. Loss function

The top 3 performance teams in both cine and mapping tasks all include the SSIM in the loss function, which aligns with the evaluation metrics of the challenge.

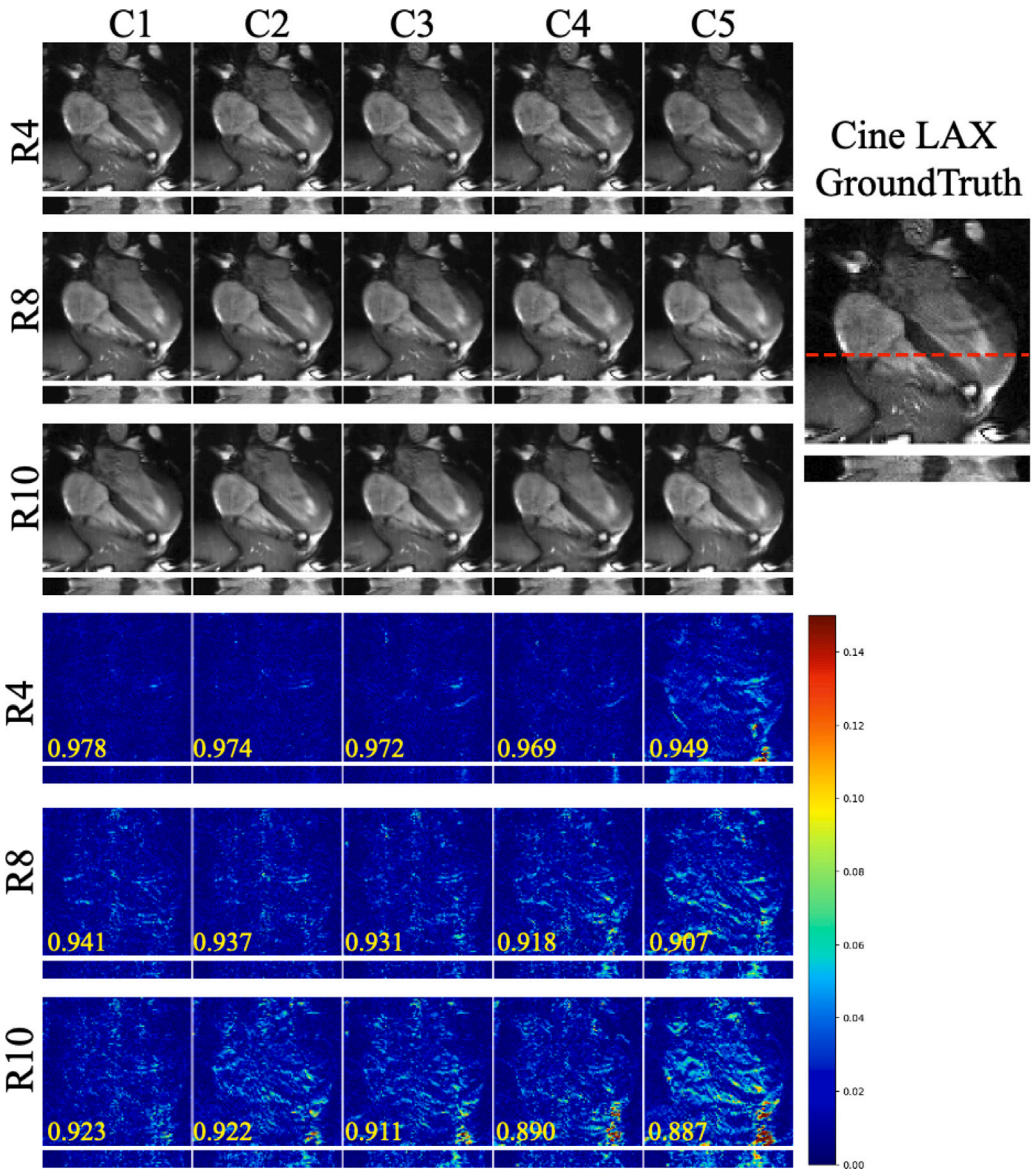

Fig. 14. Performances of the top 5 teams in cine task with LAX viewunder acceleration factors of 4, 8, and 10. The SSIM of each team is listed in the bottom left corner.

As shown in Fig. 19, for cine reconstruction, MSE is the most commonly used loss function among participants, followed closely by SSIM, MAE, and the composite loss function of MAE+SSIM, which jointly occupy the second position. Additionally, some teams have devised unique composite loss functions, such as MSE+TV, SSIM+MAE+MSE, MSE+Charbonnier, SSIM+MAE+HEFN, and SSIM+MSE+Cross Entropy.

In the case of Mapping reconstruction, MAE and SSIM+MAE are the two most frequently employed loss functions, accounting for half of the participating teams. The remaining five teams have opted for SSIM+MAE+HFEN, SSIM+MSE+Relaxometry, SSIM+MAE+MSE, and MSE+TV, respectively.

5.3.2. Backbone architecture

Several teams utilized external models as backbones, including E2E-VarNet, vSHARP, CAMP-Net, Unet, and Restormer, indicating a reliance on established architectures in Tables 7 and 8. Both the first-place winners of the two tasks utilized the E2E-VarNet (Sriram et al., 2020) architecture network as backbones. The fourth-place winner of the cine reconstruction task also use the E2E-VarNet as backbone. In addition, UNet (Falk et al., 2019) architecture is the most common backbone network for both multi-coil and single-channel reconstruction. Convolution neural networks (CNNs) remains the most commonly used backbone model by participating teams, but there are also teams that utilized the Transformer architecture.

5.3.3. Multi-scale and multi-frame strategies

The majority of teams adopted advanced strategies that emphasized the fusion of multi-scale information and multi-frame training. These approaches highlight the critical importance of integrating data across various scales and timeframes into the modeling process. By leveraging multi-scale information, teams such as TJUBIIT (C4) and IADI-IMI (C17) were able to capture a broader range of features and patterns, enhancing the model's ability to generalize and adapt to different conditions. Additionally, teams such as DIRECT(C2/M2), Clair (C3/M3), TJUBIIT (C4), imperial.cmr(M9) and Edipo(C12) incorporated multi-frame training, which allowed for a more comprehensive understanding of temporal dynamics and improved the model's performance in handling time-dependent variations and interactions within the data.

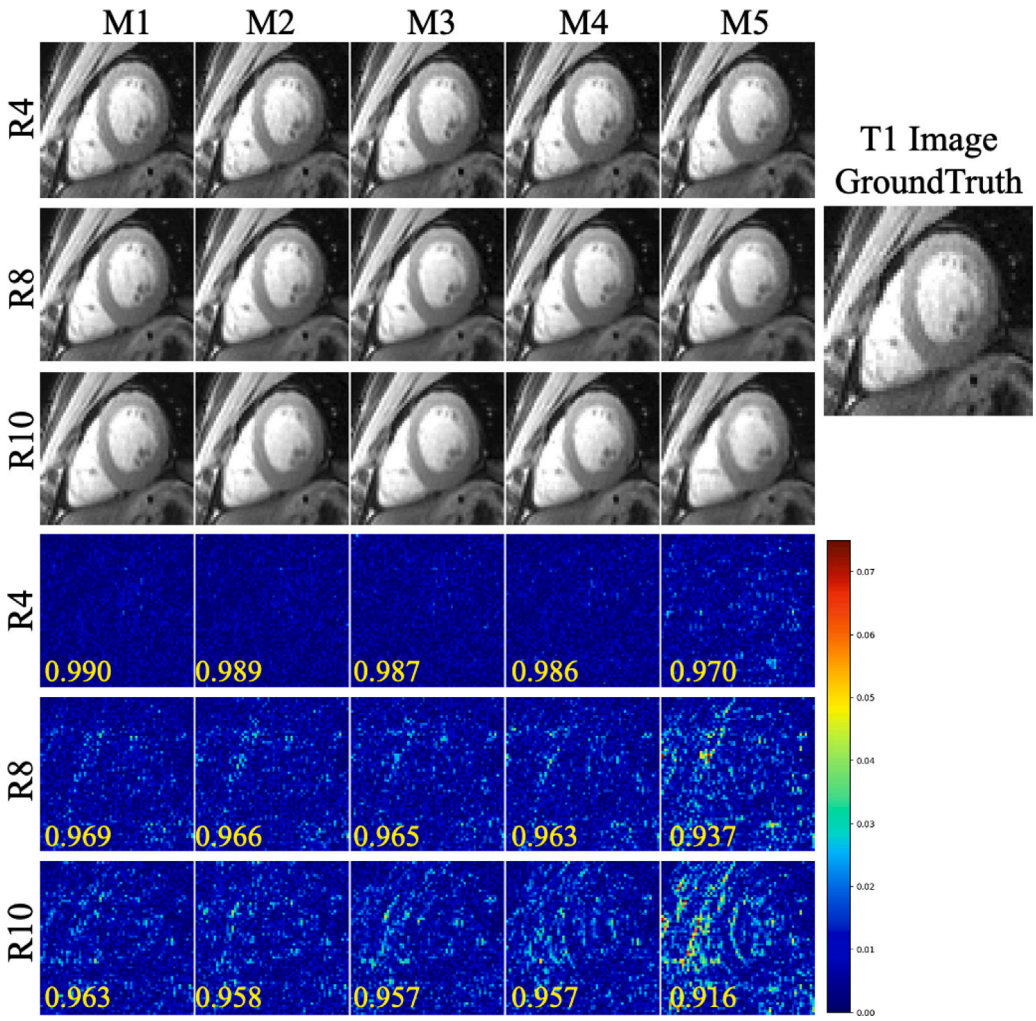

Fig. 15. Performances of the top 5 teams in T1 mapping task under acceleration factors of 4, 8, and 10. The SSIM of each team is listed in the bottom left corner.

5.3.4. Pre-processings

Regarding pre-processing, the majority of participating teams opted for normalization of dividing by the maximum value, and a few utilized the z-score normalization method. This step is particularly crucial in the context of challenge, where the original signal intensity in k-space tends to be markedly lower. Data normalization plays a pivotal role in adjusting these intensities to a more suitable scale. This adjustment is essential for the effective operation of activation functions and other components within the neural network.

5.3.5. Adherence to physical measurements

Additionally, the vast majority of participating teams incorporated the physical model, introducing a Data Consistency (DC) (Schlemper et al., 2017) term into the model to ensure consistency between the reconstructed results and the acquired data. In addition to utilizing real-collected k-space data for substitution during the reconstruction process, teams also incorporated various model-based methods into their strategies. These included advanced techniques such as ESPIRiT (Uecker et al., 2014) and JSENSE (Ying and Sheng, 2007) for coil sensitivity estimation, as well as low-rank-based iterative methods for image reconstruction.

5.4. Model complexity analysis

Recently, efficiency has garnered widespread attention in biomedical image processing challenges. The efficiency of cardiac MRI reconstruction methods is particularly crucial in clinical applications. Although efficiency does not directly impact rankings, we conducted a supplementary analysis of the complexity of the models from different teams. The testing programs submitted by participants were executed on the same Linux workstation, equipped with an Intel(R) Xeon(R) E5-2698 v4 processor (2.20 GHz base frequency, 40 cores), 256 GB of memory, and one NVIDIA® Tesla V100-DGXS-32 GB graphics processors. In competitions such as FLARE'21 (Ma et al., 2022) and ATM'22 (Zhang et al., 2023b), the runtime and maximum GPU memory consumption are among the factors considered in the ranking score calculation. Tables 9 and 10 document the maximum GPU memory consumption and inference time costs for each team in the cine reconstruction and mapping reconstruction tasks, respectively. Additionally, in Fig. 20, we compare metrics based on efficiency. C2/M2 demonstrates outstanding overall performance while maintaining a highly level of efficiency. In contrast, C1/M1 exhibits longer processing times, possibly due to the iterative algorithm employed, which may increase the inference time costs. These findings suggest us that it may be necessary to incorporate model complexity into the evaluation and development of reconstruction methods.

5.5. Ranking stability analysis

We conducted a paired t test analysis during the final ranking stage. This non-parametric test was performed to compare the distribution of SSIM values between the highest-scoring model (hellopipu) and all other models. As shown in Tables 5 and 6, the SSIM values from all other methods were statistically significantly different from those of hellopipu, with P-value levels below 0.0001 (see Fig. 21).

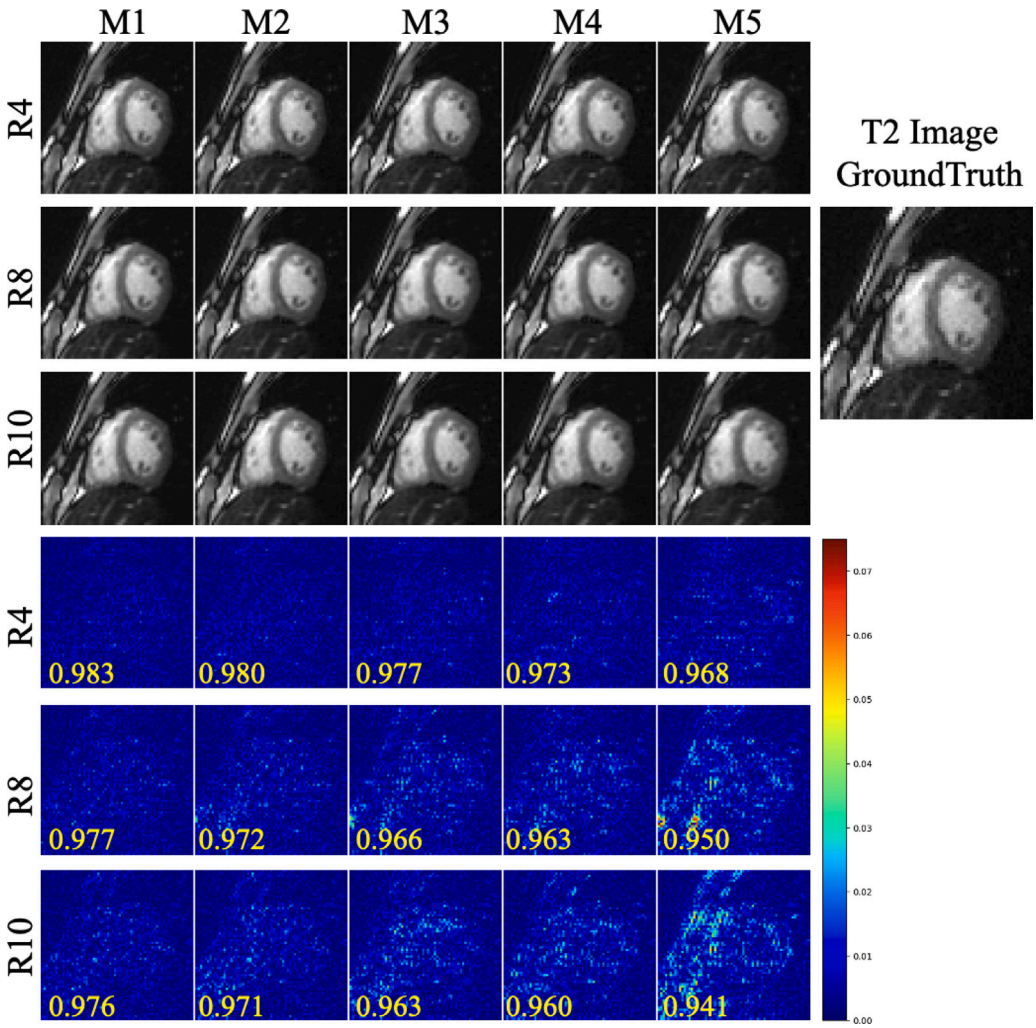

Fig. 16. Performances of the top 5 teams in T1 mapping task under acceleration factors of 4, 8, and 10. The SSIM of each team is listed in the bottom left corner.

Table 5
Statistical analysis for the cine task was performed using the paried t test. This non-parametric test compared the distribution of scores between the highest-scoring model (hellopipu) and each of the other models individually. The resulting P-values are reported for each model comparison.

Team name	hellopipu	Direct	clair	tjubiit	Imr	Jabber
P-Value	–	1.89×10^{-6}	2.96×10^{-13}	2.00×10^{-17}	5.28×10^{-14}	4.72×10^{-30}
Team Name	SkoICIG	Mataffine	OREO and CAFFE MOCHA and HCN	feiwang	Fast2501	Edipo
P-Value	3.35×10^{-27}	4.88×10^{-30}	4.72×10^{-30}	4.72×10^{-30}	4.72×10^{-30}	4.72×10^{-30}
Team Name	hkforest	tsinghuacbir	insightdcu	Lyu lab	IADI-IMI	Fzu312lab
P-Value	4.72×10^{-30}	4.72×10^{-30}	4.72×10^{-30}	4.72×10^{-30}	4.72×10^{-30}	4.72×10^{-30}

Table 6
Statistical analysis for the mapping task was performed using the paried t test. This non-parametric test compared the distribution of scores between the highest-scoring model (hellopipu) and each of the other models individually. The resulting P-values are reported for each model comparison.

Team name	hellopipu	Direct	clair	dbmapping-Mapping	Jabber	whitealbum2
P-Value	–	3.22×10^{-20}	1.15×10^{-16}	7.20×10^{-25}	9.42×10^{-35}	9.63×10^{-36}
Team Name	SkoICIG	Fast2501	imperial_cmr	IADI-IMI	sunnybrook	
P-Value	3.76×10^{-35}	6.11×10^{-37}	2.95×10^{-147}	6.11×10^{-37}	1.58×10^{-33}	

6. Discussion

The main goal of CMRxRecon is to provide an open platform for challenge and establish benchmark in the field of cardiac MRI reconstruction in the era of deep learning. The CMRxRecon Challenge has introduced the largest cardiac MRI reconstruction dataset tailored for deep learning applications to date. However, cardiac MRI reconstruction remains an open challenge for the research community. The analysis of the winning solution from 'hellopipu' reveals that while significance has been made with PSNR, SSIM, and NMSE scored 46.873, 0.990, 0.003, and 45.481, 0.987, 0.004 for cine and mapping reconstruction, respectively, the exploration into the nuanced recovery of details within the reconstructed images remains challenging, especially for higher undersampling factors. To better assess the application potential of reconstruction models, it will be necessary to introduce some patient data for testing. Specifically, based on the T1 and T2 values calculated from the reconstructed images, 'clair', who ranked the third place, has outperformed 'Direct' in terms of RMSE compared with the

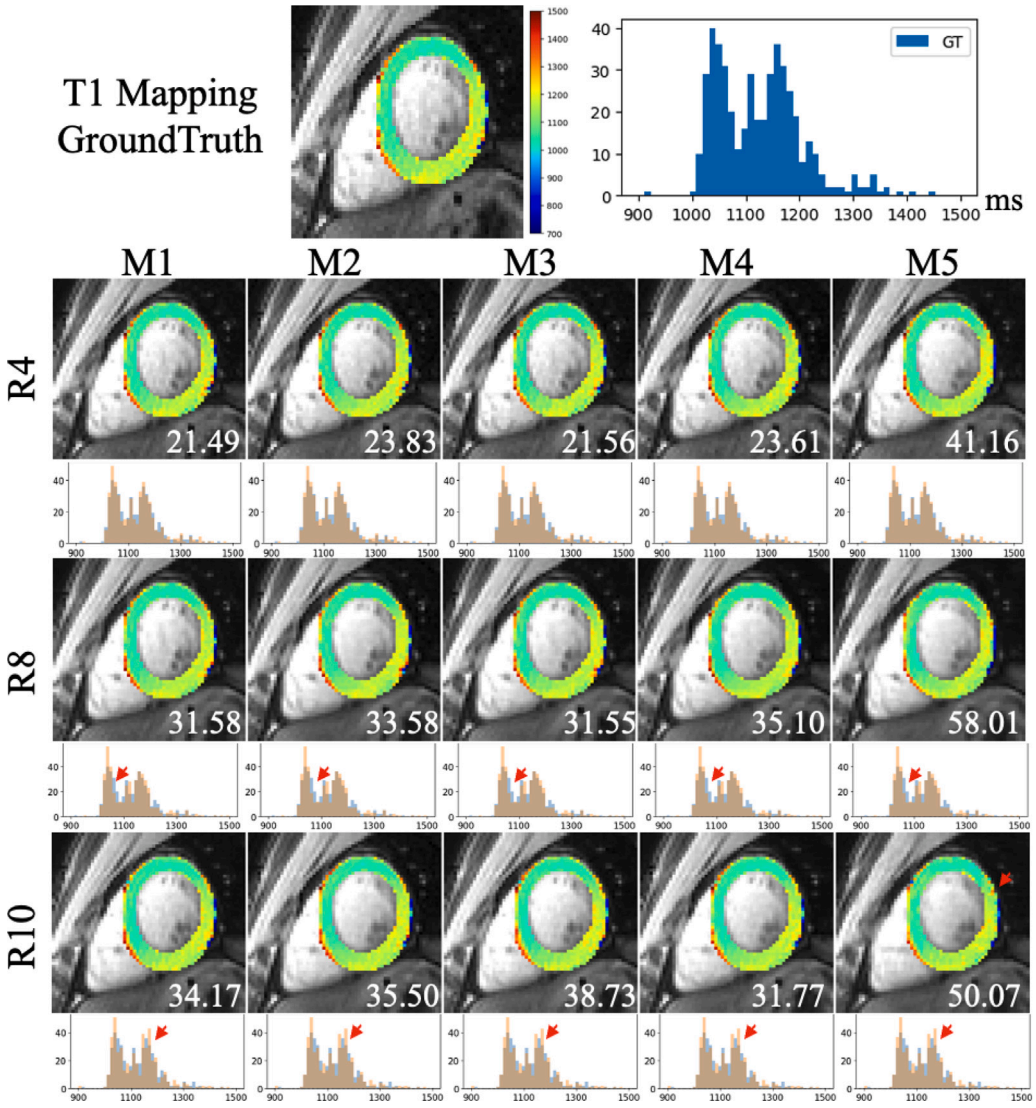

Fig. 17. The quantification performances of the myocardium are shown in T1 mapping. The histograms of the myocardium are shown. The top 5 teams in mapping tasks under acceleration factors of 4, 8, and 10. The RMSE of each team is listed in the right bottom corner.

Table 7
Characteristics of the models from all participated teams in the cardiac cine reconstruction task. Abbreviation: Multi-Coil (MC), Single-Coil (SC), Flip (F), Rotation (R), Shift (S), Data Consistency (DC), FT (Fourier Transform).

Team	Backbone	Data standardization	Data augmentation				Physical model	
			F	R	S	Others	DC	Others
C1. hellopipu	MC, E2E-VarNet (Sriram et al., 2020)	Z-score				Data balancing	✓	N/A
C2. Direct	MC, vSHARP (Yiasemis et al., 2025)	Max	✓	✓		Multiple undersampling	✓	ADMM
C3. clair	MC, CAMP-Net (Zhang et al., 2023a)	Max				N/A	✓	N/A
C4. tjubiit	MC, E2E-VarNet (Sriram et al., 2020)	Z-score	✓	✓		N/A	✓	N/A
C5. imr	MC, U-Net (Falk et al., 2019)	N/A				N/A	✓	N/A
C6. jabber	MC, U-Net (Falk et al., 2019)	Z-score	✓		✓	N/A	✓	N/A
C7. SkoICIG	MC/SC, U-Net (Falk et al., 2019)	Z-score				N/A	✓	N/A
C8. Mataffine	MC/SC, U-Net (Falk et al., 2019)	N/A				N/A		N/A
C9. OREO	SC, Transformer (Vaswani et al., 2017)	Max			✓	N/A	✓	N/A
C10. feiwang	MC, MoDL (Aggarwal et al., 2018)	Max				N/A	✓	FISTA
C11. Fast2501	MC/SC, U-Net (Falk et al., 2019)	Max	✓			Multiple undersampling	✓	ESPIRiT
C12. Edipo	SC, CRNN (Qin et al., 2018)	N/A				N/A	✓	N/A
C13. hkforest	MC/SC, DDPM (Ho et al., 2020)	Max				N/A	✓	N/A
C14. tsinghuacbir	SC, CRNN (Qin et al., 2018)	Max	✓			N/A	✓	N/A
C15. insightdcu	SC, U-Net (Falk et al., 2019)	N/A				N/A		N/A
C16. lyu lab	MC, NAFNet (Chu et al., 2022)	Max				N/A	✓	N/A
C17. IADI-IMI	MC, INN (Müller et al., 2022)	Max				N/A	✓	JSENSE
C18. Fzu312lab	SC, U-Net (Falk et al., 2019)	Max				N/A		N/A

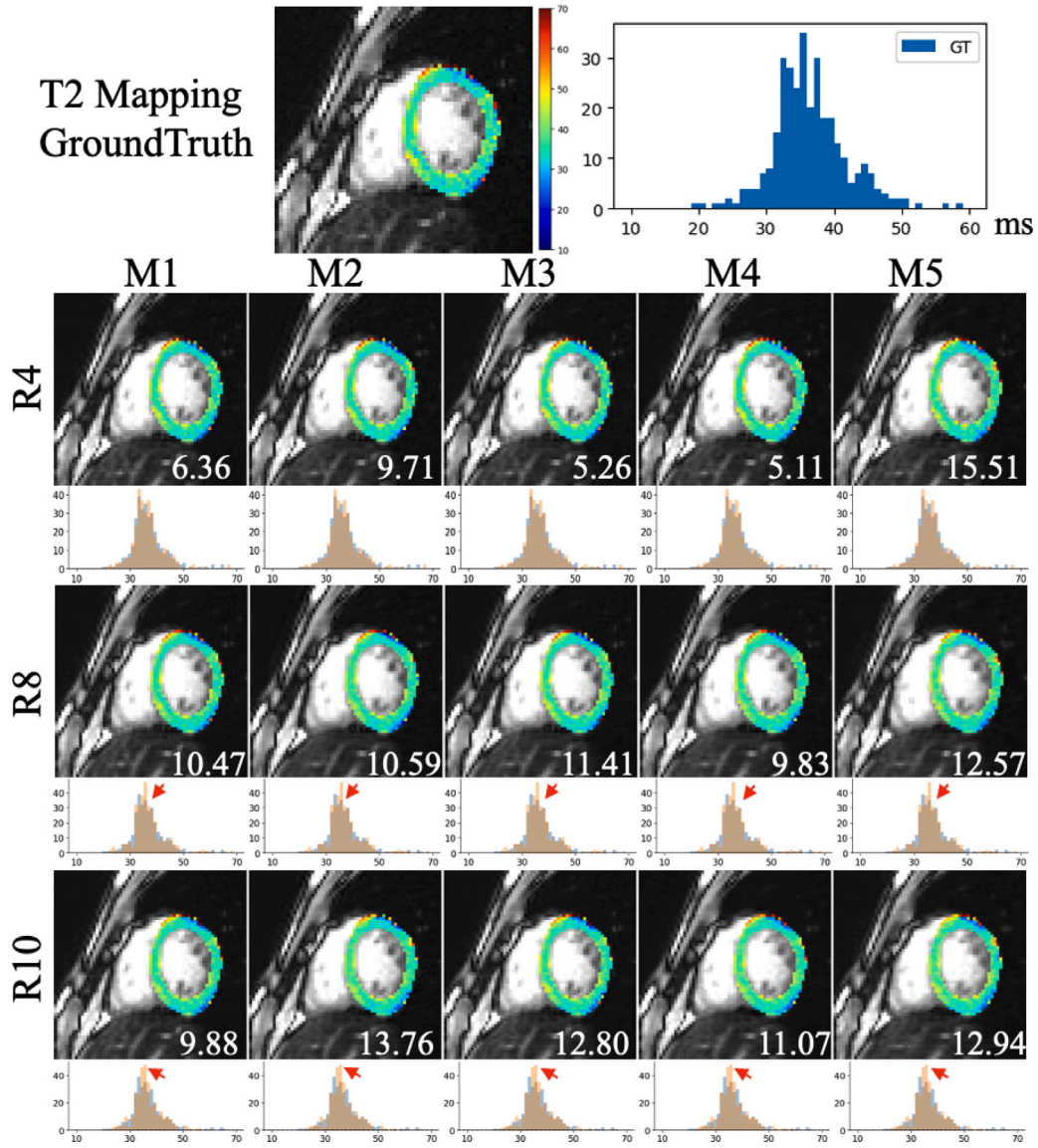

Fig. 18. The quantification performances of the myocardium are shown in T2 mapping. The histograms of the myocardium are shown. The top 5 teams in mapping tasks under acceleration factors of 4, 8, and 10. The RMSE of each team is listed in the right bottom corner.

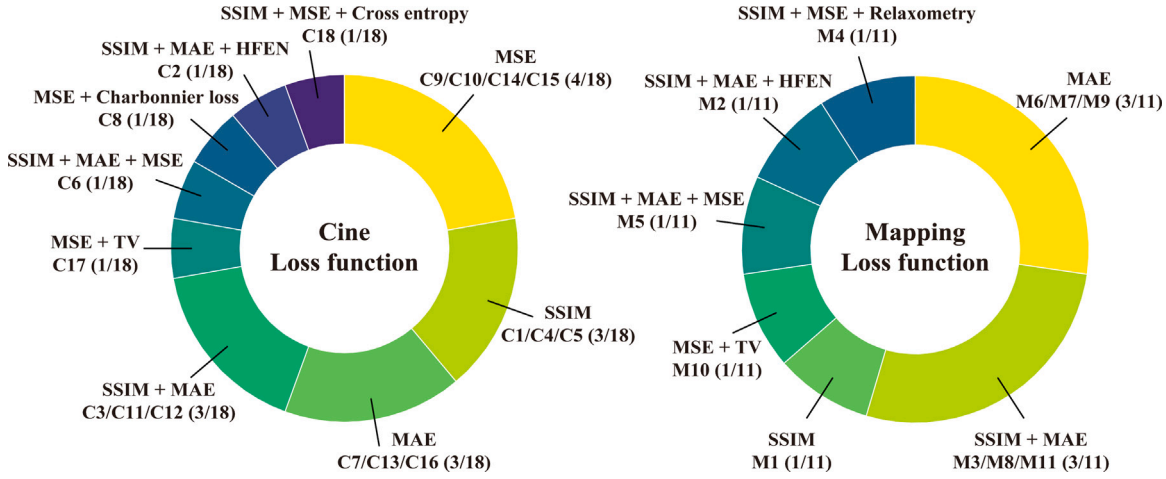

Fig. 19. Loss function adapted by all ranked teams in the cardiac cine (left) and mapping (right) reconstruction tasks.

Table 8
Characteristics of the models from all participated teams in the cardiac mapping reconstruction task. Abbreviation: Multi-Coil (MC), Single-Coil (SC), Flip (F), Rotation (R), Shift (S), Data Consistency (DC), FT (Fourier Transform).

Team	Backbone	Data standardization	Data augmentation				Physical model	
			F	R	S	Others	DC	Others
M1. hellopipu	MC, E2E-VarNet (Sriram et al., 2020)	Z-score				Data balancing	✓	N/A
M2. Direct	MC, vSHARP (Yiasemis et al., 2025)	Max	✓	✓		Multiple undersampling	✓	ADMM
M3. clair	MC, CAMP-Net (Zhang et al., 2023a)	Max				N/A	✓	N/A
M4. dbmapping	MC, U-Net (Falk et al., 2019)	Min-Max	✓	✓	✓	Gaussian noise addition	✓	Relaxometry
M5. jabber	MC, U-Net (Falk et al., 2019)	Z-score	✓		✓	N/A	✓	N/A
M6. whitealbum2	MC/SC, MedNeXt (Roy et al., 2023)	Z-score				N/A		N/A
M7. SkoICIG	MC/SC, U-Net (Falk et al., 2019)	Z-score				N/A	✓	N/A
M8. Fast2501	MC/SC, U-Net (Falk et al., 2019)	Max	✓			Multiple undersampling	✓	ESPIRiT
M9. imperial_cmr	MC/SC, MoDL (Aggarwal et al., 2018)	Max				Multiple undersampling	✓	ESPIRiT
M10. IADI-IMI	MC, INN (Müller et al., 2022)	Max				N/A	✓	JSENSE
M11. sunnybrook	MC, U-Net (Falk et al., 2019)	Z-score				N/A	✓	Low-rank

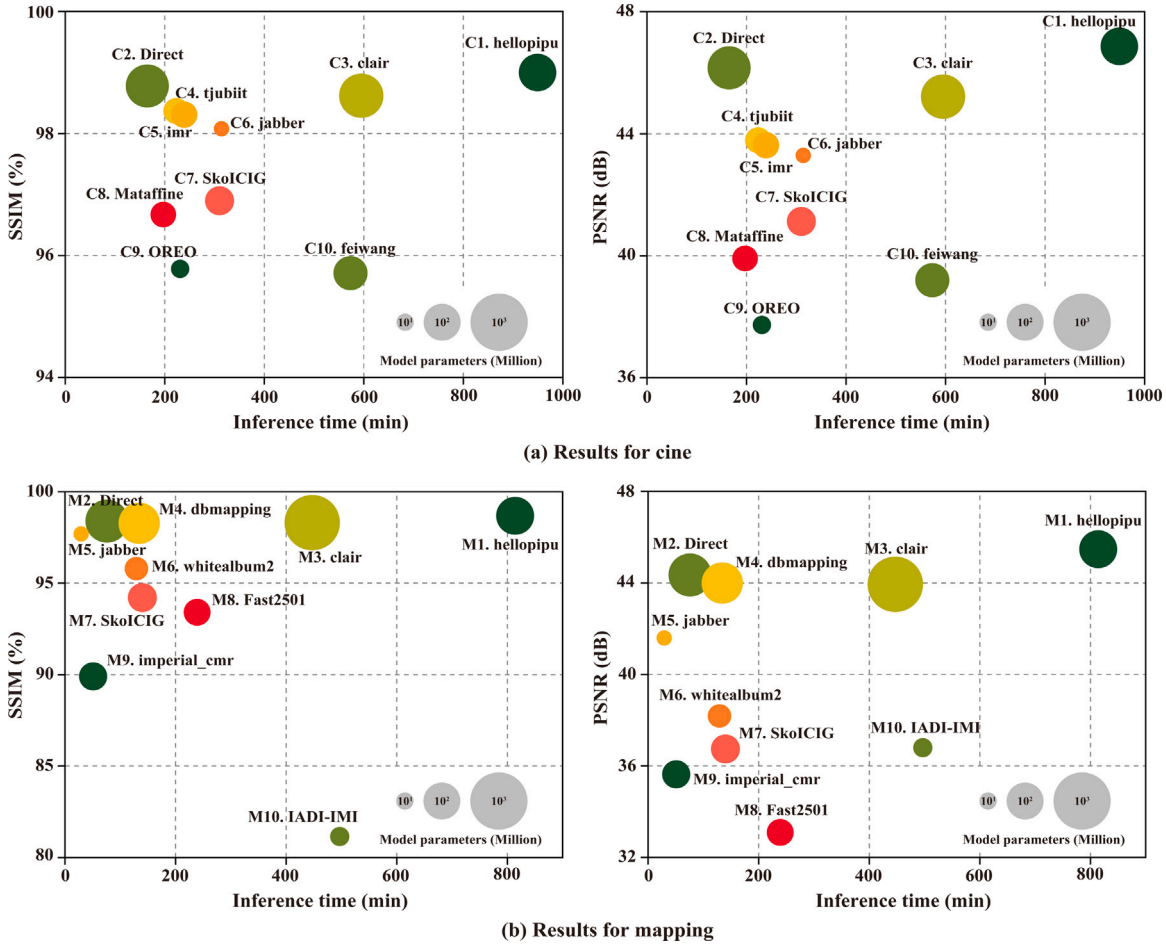

Fig. 20. Comparison of top 10 teams on the inference times and evaluation metrics. The larger markers indicate more model parameters.

ground-truth mapping values 4. A 10× acceleration method can meet clinical requirements and outperforms SENSE/GRAPPA in the machine, which achieves a maximum of 3×. For atrial fibrillation or arrhythmias, an 8∼10× acceleration seems feasible using the top three methods.

As shown in Tables 9 and 10, the inference time of hellopipu's model is about 7 min and 6 min per case for cine and mapping tasks, respectively, since hellopipu employs models with 111M parameters for the cine reconstruction and 121M parameters for the mapping reconstruction. While not the highest parameter count reported, the model's complexity could contribute to longer processing times. However, the inference time does not solely depend on the model size, as demonstrated by other teams with larger models achieving faster inference times. The CPU memory usage by 'hellopipu' is relatively moderate in cine reconstruction and significantly lower in mapping reconstruction compared to the highest CPU memory usage reported. However, GPU memory usage is among the highest for both tasks, since they have incorporated the large foundation model as the Prompt Block. Moreover, we just use one GPU in the testing stage. Ensuring efficient inference when restricted to using just one GPU centers around maximizing the computational efficiency and throughput of the available hardware. This process involves a combination of optimizing the model itself and leveraging the specific capabilities and features of the GPU to full effect. Therefore, the trade-off between the reconstruction performance and the model's extrapolation time remains a promising research direction.

In a post-event survey, suggestions for future improvements to the CMR reconstruction challenge were received from 28 participants. A

Table 9
Computational consumption and reconstruction performances of top 10 teams in the cardiac cine reconstruction task.

Team	CPU memory	GPU memory	Model para.	Inference time
C1. hellopipu	21.97 GB	15.78 GB	111 M	15 h 49 min
C2. Direct	48.22 GB	18.3 GB	225 M	2 h 45 min
C3. clair	145.22 GB	2.88 GB	264 M	9 h 55 min
C4. tjubiit	119.31 GB	4.75 GB	27 M	3 h 43 min
C5. imr	22.18 GB	9.18 GB	28 M	3 h 59 min
C6. jabber	114 GB	3.15 GB	7 M	5 h 14 min
C7. SkoICIG	33.85 GB	9.96 GB	38 M	5 h 10 min
C8. Mataffine	23.5 GB	6.87 GB	25 M	3 h 17 min
C9. OREO	19.59 GB	3.97 GB	10 M	3 h 51 min
C10. feiwang	37.98 GB	4.21 GB	74 M	9h 43 min

Table 10
Computational consumption and reconstruction performances of top 10 teams in the cardiac mapping reconstruction task.

Team	CPU memory	GPU memory	Model para.	Inference time
M1. hellopipu	10.2 GB	18.35 GB	121 M	13 h 34 min
M2. Direct	23.6 GB	18.08 GB	225 M	1 h 16 min
M3. clair	50.34 GB	5.64 GB	1100 M	7 h 27 min
M4. dbmapping	29.07 GB	14.09 GB	181 M	2 h 14 min
M5. jabber	48.55 GB	4.2 GB	7 M	30 min
M6. whitealbum2	159.52 GB	3.46 GB	19 M	2 h 9 min
M7. SkoICIG	17.12 GB	5.19 GB	38 M	2 h 20 min
M8. Fast2501	20.78 GB	1.94 GB	30 M	3 h 59 min
M9. imperial_cmr	46.26 GB	15.12 GB	35 M	51 min
M10. IADI-IMI	8.56 GB	3.3 GB	11 M	8 h 17 min

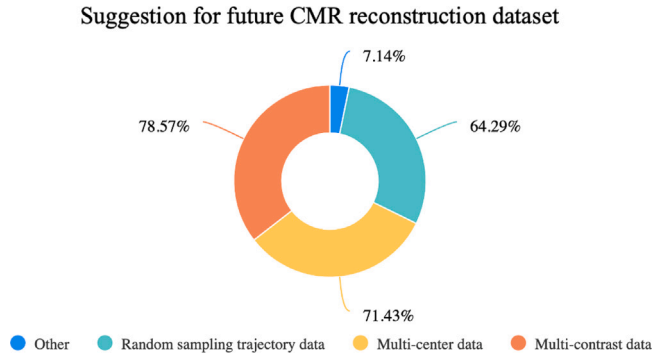

Fig. 21. Suggestions for future CMR reconstruction dataset from 28 participants in a post-event survey.

total of 78.58% of teams expressed a desire for k-space data with more contrast in future challenges. Additionally, 71.43% of teams recommended the inclusion of multi-center cardiac data to enhance the diversity of the dataset. Furthermore, 64.29% of teams hoped for the availability of random sampling trajectory data, contributing to a more comprehensive coverage of cardiac images under different scenarios. The remaining 7.14% proposed other content. These suggestions will contribute to optimizing future CMR challenges as well as public datasets to better align with the needs from the participants. Our next step involves expanding in the following areas as we continue to organize several CMR reconstruction challenges in the future:

Providing diverse sampling trajectories. Instead of applying uniform sampling along the time dimension, better strategy should follow random sampling, hence maximizing the information along the time dimension. Such a refined strategy not only enhances the efficiency of image acquisition but also contributes significantly to the integration of CMR imaging into clinical workflows.

Expanding clinical generalization through multi-center and disease-specific Data. Our current dataset (Wang et al., 2023a) predominantly consists of CMR data from healthy volunteers, obtained using equipment from a single vendor in a single-center setting. Recognizing the limitations this imposes on the generalizability of data-driven models, we are supposed to include a diverse range of pathological conditions and data from multiple vendors and centers. This comprehensive inclusion will pave the way for the development of robust models capable of accommodating the variability inherent in clinical environments, thereby enhancing the reliability and applicability of CMR across different patient populations and diagnostic contexts.

Finding advanced evaluations for performance benchmarking. We leveraged the SSIM as our evaluation for benchmarking in the current challenge, which enables a precise comparison between the reconstructed images and fully-sampled images. However, we acknowledge the necessity of a more encompassing evaluation framework that goes beyond mere image quality, such as inference time and the generation of further parametric maps. Inference time, indicative of the speed at which the models reconstruct images, is paramount in clinical settings where timely diagnostics are critical. Moreover, the development and analysis of parametric maps extend our capabilities beyond anatomical imaging, offering insights into the functional and tissue characteristics of the myocardium.

Trustworthy reconstruction on multi-contrast CMR imaging. We aim to obtain data with more contrasts to achieve reliable and accurate reconstructions. The complexity and diversity of CMR scans in real-world applications, involving various contrasts, sampling trajectories, scan orientations, equipment vendors, and disease types, present a great challenge for existing AI-based reconstruction methods, which are usually developed for only one or a few specific scanning settings. In practice, there are often inevitable domain mismatches between the training data and target data, due to the diversities listed above (Ouyang et al., 2019; Knoll et al., 2019; Yang et al., 2023). Therefore, building and validating universal and robust reconstruction models for handling these diversities remains a critical technical challenge for multi-parametric CMR imaging (Ouyang et al., 2019; Liu et al., 2021; Wang et al., 2023c; Tänzer et al., 2023). To accomplish this, people may leverage a universal pre-trained reconstruction model to handle the heterogeneity and intricacies of multi-contrast imaging, ensuring high fidelity and trustworthiness in reconstructed results.

7. Conclusion

The CMRxRecon challenge offers a benchmark dataset comprising multi-contrast, multi-view, and multi-coil raw k-space data with manually annotated labels for cardiac anatomical structures. This dataset enables the research community to actively contribute to the development of deep learning-based cardiac MRI reconstruction algorithms. Our paper provides a comprehensive overview of the challenge design, presents a summary of the submitted results, reviews the employed methods, and offers an in-depth discussion that aims to inspire future advancements in cardiac MRI reconstruction models. The summary highlights effective strategies observed in cardiac MRI reconstruction, including backbone architecture, loss function, pre-processing techniques, physical modeling, and model complexity, providing valuable insights for further advancements in this field.

CRediT authorship contribution statement

Jun Lyu: Writing – original draft, Conceptualization. **Chen Qin:** Writing – original draft, Conceptualization. **Shuo Wang:** Supervision, Project administration. **Fanwen Wang:** Writing – original draft, Methodology. **Yan Li:** Formal analysis, Data curation. **Zi Wang:** Investigation, Formal analysis. **Kunyuan Guo:** Formal analysis, Data curation. **Cheng Ouyang:** Investigation, Formal analysis. **Michael Tänzer:** Formal analysis, Data curation. **Meng Liu:** Investigation, Formal analysis. **Longyu Sun:** Formal analysis, Data curation. **Mengting Sun:** Investigation, Formal analysis. **Qing Li:** Validation, Investigation. **Zhang Shi:** Resources, Data curation. **Sha Hua:** Resources, Data curation. **Hao Li:**

Formal analysis, Data curation. **Zhensen Chen:** Investigation, Formal analysis. **Zhenlin Zhang:** Investigation, Formal analysis. **Bingyu Xin:** Investigation, Formal analysis. **Dimitris N. Metaxas:** Formal analysis, Data curation. **George Yiasemis:** Investigation, Formal analysis. **Jonas Teuwen:** Formal analysis, Data curation. **Liping Zhang:** Investigation, Formal analysis. **Weitian Chen:** Formal analysis, Data curation. **Yidong Zhao:** Conceptualization, Writing – review & editing. **Qian Tao:** Conceptualization, Writing – review & editing. **Yanwei Pang:** Investigation, Data curation. **Xiaohan Liu:** Investigation, Formal analysis. **Artem Razumov:** Investigation, Formal analysis. **Dmitry V. Dylov:** Formal analysis, Data curation. **Quan Dou:** Investigation, Data curation. **Kang Yan:** Investigation, Formal analysis. **Yuyang Xue:** Formal analysis, Data curation. **Yuning Du:** Formal analysis, Data curation. **Julia Dietlmeier:** Investigation, Formal analysis. **Carles Garcia-Cabrera:** Investigation, Formal analysis. **Ziad Al-Haj Hemidi:** Formal analysis, Data curation. **Nora Vogt:** Investigation, Data curation. **Ziqiang Xu:** Formal analysis, Data curation. **Yajing Zhang:** Formal analysis, Data curation. **Ying-Hua Chu:** Investigation, Formal analysis. **Weibo Chen:** Investigation, Formal analysis. **Wenjia Bai:** Investigation, Data curation. **Xiahai Zhuang:** Investigation, Formal analysis. **Jing Qin:** Investigation, Formal analysis. **Lianming Wu:** Investigation, Data curation. **Guang Yang:** Formal analysis, Data curation. **Xiaobo Qu:** Investigation, Formal analysis. **He Wang:** Investigation, Data curation. **Chengyan Wang:** Investigation, Formal analysis, Data curation.

Declaration of competing interest

The authors declare that they have no known competing financial interests or personal relationships that could have appeared to influence the work reported in this paper.

Acknowledgments

This work was supported in part by the National Natural Science Foundation of China under Grants 62371413, 62331021, and 62122064, in part by Yantai Basic Research Key Project, China 2023JCYJ041, in part by the Youth Innovation Science and Technology Support Program of Shandong Provincial, China under Grant 2023KJ239, in part by the Youth Program of Natural Science Foundation of Shandong Province ZR2024QF001, in part by the Natural Science Foundation of Fujian Province of China under Grant 2023J02005, in part by the President Fund of Xiamen University, China under Grant 20720220063, in part by the EPSRC, UK Grants (TrustMRI: EP/X039277/1), in part by the UKRI Centre for Doctoral Training in AI for Healthcare, Imperial College London, UK under Grant EP/S023283/1, in part by the ERC IMI (101005122), the H2020 (952172), the MRC (MC/PC/21013), the Royal Society, United Kingdom (IEC\NSFC\211235), the NVIDIA Academic Hardware Grant Program, the SABER project supported by Boehringer Ingelheim Ltd, NIHR Imperial Biomedical Research Centre (RDA01), in part by the Wellcome Leap Dynamic Resilience, UKRI guarantee funding for Horizon Europe MSCA Postdoctoral Fellowships (EP/Z002206/1), in part by the UKRI Future Leaders Fellowship (MR/V023799/1), in part by the National Institutes of Health (NIH), United States grant 7R01HL148788-03, the Royal Academy of Engineering and the Research Chairs and Senior Research Fellowships scheme (grant RCSRF1819\8\25), and the UK's Engineering and Physical Sciences Research Council (EPSRC) support via grant EP/X017680/1, in part by the China Scholarship Council under grant 202306310177, in part by the Shanghai Municipal Science and Technology Major Project (No.2023SHZD2X02A05), and in part by the Shanghai Rising-Star Program (No.24QA2703300). The computations in this research were performed using the CFFF platform of Fudan University.

Data availability

Data will be made available on request.

References

Aggarwal, H.K., Mani, M.P., Jacob, M., 2018. MoDL: Model-based deep learning architecture for inverse problems. IEEE Trans. Med. Imaging 38 (2), 394–405.

Akçakaya, M., Moeller, S., Weingärtner, S., Uğurbil, K., 2019. Scan-specific robust artificial-neural-networks for k-space interpolation (RAKI) reconstruction: Database-free deep learning for fast imaging. Magn. Reson. Med. 81 (1), 439–453.

Al-Haj Hemidi, Z., Vogt, N., Quillien, L., Weihsbach, C., Heinrich, M.P., Oster, J., 2023. CineJENSE: Simultaneous cine MRI image reconstruction and sensitivity map estimation using neural representations. In: International Workshop on Statistical Atlases and Computational Models of the Heart. Springer, pp. 467–478.

Beauferris, Y., Teuwen, J., Karkalousos, D., Moriakov, N., Caan, M., Yiasemis, G., Rodrigues, L., Lopes, A., Pedrini, H., Rittner, L., Dannecker, M., Studenyak, V., Gröger, F., Vyas, D., Faghih-Roohi, S., Kumar Jethi, A., Chandra Raju, J., Sivaprakasam, M., Lasby, M., Nogovitsyn, N., Loos, W., Frayne, R., Souza, R., 2022. Multi-coil MRI reconstruction challenge—Assessing brain MRI reconstruction models and their generalizability to varying coil configurations. Front. Neurosci. 16, http://dx.doi.org/10.3389/fnins.2022.919186, URL https://www.frontiersin.org/journals/neuroscience/articles/10.3389/fnins.2022.919186.

Bernard, O., Lalande, A., Zotti, C., Cervenansky, F., Yang, X., Heng, P.A., Cetin, I., Lekadir, K., Camara, O., Ballester, M.A.G., et al., 2018. Deep learning techniques for automatic MRI cardiac multi-structures segmentation and diagnosis: is the problem solved? IEEE Trans. Med. Imaging 37 (11), 2514–2525.

Bilecen, B.B., Ayazoglu, M., 2023. Bicubic++: Slim, slimmer, slimmest-designing an industry-grade super-resolution network. In: Proceedings of the IEEE/CVF Conference on Computer Vision and Pattern Recognition. pp. 1623–1632.

Biswas, S., Aggarwal, H.K., Jacob, M., 2019. Dynamic MRI using model-based deep learning and SToRM priors: MoDL-SToRM. Magn. Reson. Med. 82 (1), 485–494.

Campello, V.M., Gkontra, P., Izquierdo, C., Martin-Isla, C., Sojoudi, A., Full, P.M., Maier-Hein, K., Zhang, Y., He, Z., Ma, J., et al., 2021. Multi-centre, multi-vendor and multi-disease cardiac segmentation: the M&Ms challenge. IEEE Trans. Med. Imaging 40 (12), 3543–3554.

Chen, C., Liu, Y., Schniter, P., Tong, M., Zareba, K., Simonetti, O., Potter, L., Ahmad, R., 2020. OCMR (v1. 0)–open-access multi-coil k-space dataset for cardiovascular magnetic resonance imaging. arXiv preprint arXiv:2008.03410.

Chu, X., Chen, L., Yu, W., 2022. NAFSSR: Stereo image super-resolution using nafnet. In: Proceedings of the IEEE/CVF Conference on Computer Vision and Pattern Recognition. pp. 1239–1248.

Chung, H., Ye, J.C., 2022. Score-based diffusion models for accelerated MRI. Med. Image Anal. 80, 102479.

Donoho, D.L., 2006. Compressed sensing. IEEE Trans. Inform. Theory 52 (4), 1289–1306.

Duan, J., Schlemper, J., Qin, C., Ouyang, C., Bai, W., Biffi, C., Bello, G., Statton, B., O'regan, D.P., Rueckert, D., 2019. VS-net: Variable splitting network for accelerated parallel MRI reconstruction. In: Medical Image Computing and Computer Assisted Intervention–MICCAI 2019: 22nd International Conference, Shenzhen, China, October 13–17, 2019, Proceedings, Part IV 22. Springer, pp. 713–722.

El-Rewaidy, H., Fahmy, A.S., Pashakhanloo, F., Cai, X., Kucukseymen, S., Csecs, I., Neisius, U., Haji-Valizadeh, H., Menze, B., Nezafat, R., 2022. Multi-domain convolutional neural network (md-cnn) for radial reconstruction of dynamic cardiac mri. Magnetic Resonance in Medicine 85 (3), 1195–1208.

Eyre, K., Lindsay, K., Razzaq, S., Chetrit, M., Friedrich, M., 2022. Simultaneous multiparametric acquisition and reconstruction techniques in cardiac magnetic resonance imaging: basic concepts and status of clinical development. Front. Cardiovasc. Med. 9, 953823.

Fabian, Z., Tinaz, B., Soltanolkotabi, M., 2022. Humus-net: Hybrid unrolled multi-scale network architecture for accelerated mri reconstruction. Adv. Neural Inf. Process. Syst. 35, 25306–25319.

Falk, T., Mai, D., Bensch, R., Çiçek, Ö., Abdulkadir, A., Marrakchi, Y., Böhm, A., Deubner, J., Jäckel, Z., Seiwald, K., et al., 2019. U-net: deep learning for cell counting, detection, and morphometry. Nature Methods 16 (1), 67–70.

Feng, J., Feng, R., Wu, Q., Zhang, Z., Zhang, Y., Wei, H., 2022. Spatiotemporal implicit neural representation for unsupervised dynamic MRI reconstruction. arXiv preprint arXiv:2301.00127.

Feng, R., Wu, Q., Feng, J., She, H., Liu, C., Zhang, Y., Wei, H., 2023. IMJENSE: Scan-specific implicit representation for joint coil sensitivity and image estimation in parallel MRI. IEEE Trans. Med. Imaging.

Fukushima, M., 1992. Application of the alternating direction method of multipliers to separable convex programming problems. Comput. Optim. Appl. 1, 93–111.

Griswold, M.A., Jakob, P.M., Heidemann, R.M., Nittka, M., Jellus, V., Wang, J., Kiefer, B., Haase, A., 2002. Generalized autocalibrating partially parallel acquisitions (GRAPPA). Magn. Reson. Med.: Off. J. Int. Soc. Magn. Reson. Med. 47 (6), 1202–1210.

Güngör, A., Dar, S.U., Öztürk, c., Korkmaz, Y., Bedel, H.A., Elmas, G., Ozbey, M., Çukur, T., 2023. Adaptive diffusion priors for accelerated MRI reconstruction. Med. Image Anal. 102872.

Guo, R., El-Rewaidy, H., Assana, S., Cai, X., Amyar, A., Chow, K., Bi, X., Yankama, T., Cirillo, J., Pierce, P., et al., 2022. Accelerated cardiac T1 mapping in four heartbeats with inline MyoMapNet: a deep learning-based T1 estimation approach. J. Cardiovasc. Magn. Reson. 24 (1), 1–15.

Hammernik, K., Klatzer, T., Kobler, E., Recht, M.P., Sodickson, D.K., Pock, T., Knoll, F., 2018. Learning a variational network for reconstruction of accelerated mri data. Magn. Reson. Med. 79 (6), 3055–3071.

Hammernik, K., Schlemper, J., Qin, C., Duan, J., Summers, R.M., Rueckert, D., 2021. Systematic evaluation of iterative deep neural networks for fast parallel MRI reconstruction with sensitivity-weighted coil combination. Magn. Reson. Med. 86 (4), 1859–1872.

Hauptmann, A., Arridge, S., Lucka, F., Muthurangu, V., Steeden, J.A., 2019. Real-time cardiovascular MR with spatio-temporal artifact suppression using deep learning–proof of concept in congenital heart disease. Magn. Reson. Med. 81 (2), 1143–1156.

Ho, J., Jain, A., Abbeel, P., 2020. Denoising diffusion probabilistic models. In: Advances in Neural Information Processing Systems. pp. 6840–6851.

Huang, W., Ke, Z., Cui, Z.-X., Cheng, J., Qiu, Z., Jia, S., Ying, L., Zhu, Y., Liang, D., 2021. Deep low-rank plus sparse network for dynamic MR imaging. Med. Image Anal. 73, 102190.

Huang, W., Li, H.B., Pan, J., Cruz, G., Rueckert, D., Hammernik, K., 2023. Neural implicit k-space for binning-free non-cartesian cardiac MR imaging. In: International Conference on Information Processing in Medical Imaging. Springer, pp. 548–560.

Huang, Q., Yang, D., Wu, P., Qu, H., Yi, J., Metaxas, D., 2019. MRI reconstruction via cascaded channel-wise attention network. In: 2019 IEEE 16th International Symposium on Biomedical Imaging. ISBI 2019, IEEE, pp. 1622–1626.

Ismail, T.F., Strugnell, W., Coletti, C., Božić-Iven, M., Weingaertner, S., Hammernik, K., Correia, T., Kuestner, T., 2022. Cardiac MR: from theory to practice. Front. Cardiovasc. Med. 9, 826283.

Jerosch-Herold, M., Coelho-Filho, O., 2022. Cardiac MRI T1 and T2 mapping: A new crystal ball? Radiology 305 (2), 327–328.

Knoll, F., Hammernik, K., Kobler, E., Pock, T., Recht, M.P., Sodickson, D.K., 2019. Assessment of the generalization of learned image reconstruction and the potential for transfer learning. Magn. Reson. Med. 81 (1), 116–128.

Kofler, A., Dewey, M., Schaeffter, T., Wald, C., Kolbitsch, C., 2019. Spatio-temporal deep learning-based undersampling artefact reduction for 2D radial cine MRI with limited training data. IEEE Trans. Med. Imaging 39 (3), 703–717.

Kuzmina, E., Razumov, A., Rogov, O.Y., Adalsteinsson, E., White, J., Dylov, D.V., 2022. Autofocusing+: Noise-resilient motion correction in magnetic resonance imaging. In: International Conference on Medical Image Computing and Computer-Assisted Intervention. Springer, pp. 365–375.

Lalande, A., Chen, Z., Pommier, T., Decourselle, T., Qayyum, A., Salomon, M., Ginhac, D., Skandarani, Y., Boucher, A., Brahim, K., et al., 2022. Deep learning methods for automatic evaluation of delayed enhancement-MRI. The results of the EMIDEC challenge. Med. Image Anal. 79, 102428.

Li, D., Shi, X., Zhang, Y., Cheung, K.C., See, S., Wang, X., Qin, H., Li, H., 2023. A simple baseline for video restoration with grouped spatial-temporal shift. In: Proceedings of the IEEE/CVF Conference on Computer Vision and Pattern Recognition. pp. 9822–9832.

Li, L., Zimmer, V.A., Schnabel, J.A., Zhuang, X., 2022. AtrialJSQnet: A new framework for joint segmentation and quantification of left atrium and scars incorporating spatial and shape information. Med. Image Anal. 76, 102303.

Liu, X., Wang, J., Liu, F., Zhou, S.K., 2021. Universal undersampled mri reconstruction. In: Medical Image Computing and Computer Assisted Intervention–MICCAI 2021: 24th International Conference, Strasbourg, France, September 27–October 1, 2021, Proceedings, Part VI 24. Springer, pp. 211–221.

Lustig, M., Donoho, D.L., Santos, J.M., Pauly, J.M., 2008. Compressed sensing MRI. IEEE Signal Process. Mag. 25 (2), 72–82.

Lv, J., Chen, K., Yang, M., Zhang, J., Wang, X., 2018. Reconstruction of undersampled radial free-breathing 3D abdominal MRI using stacked convolutional auto-encoders. Med. Phys. 45 (5), 2023–2032.

Lv, J., Li, G., Tong, X., Chen, W., Huang, J., Wang, C., Yang, G., 2021a. Transfer learning enhanced generative adversarial networks for multi-channel MRI reconstruction. Comput. Biol. Med. 134, 104504.

Lv, J., Wang, P., Tong, X., Wang, C., 2020. Parallel imaging with a combination of sensitivity encoding and generative adversarial networks. Quant. Imaging Med. Surg. 10 (12), 2260.

Lv, J., Wang, C., Yang, G., 2021b. PIC-GAN: a parallel imaging coupled generative adversarial network for accelerated multi-channel MRI reconstruction. Diagnostics 11 (1), 61.

Lv, J., Zhu, J., Yang, G., 2021c. Which GAN? A comparative study of generative adversarial network-based fast MRI reconstruction. Phil. Trans. R. Soc. A 379 (2200), 20200203.

Lyu, J., Li, G., Wang, C., Qin, C., Wang, S., Dou, Q., Qin, J., 2023a. Region-focused multi-view transformer-based generative adversarial network for cardiac cine MRI reconstruction. Med. Image Anal. 85, 102760.

Lyu, J., Li, Y., Yan, F., Chen, W., Wang, C., Li, R., 2023b. Multi-channel GAN–based calibration-free diffusion-weighted liver imaging with simultaneous coil sensitivity estimation and reconstruction. Front. Oncol. 13, 1095637.

Lyu, J., Sui, B., Wang, C., Dou, Q., Qin, J., 2023c. Adaptive feature aggregation based multi-task learning for uncertainty-guided semi-supervised medical image segmentation. Expert Syst. Appl. 232, 120836.

Lyu, J., Sui, B., Wang, C., Tian, Y., Dou, Q., Qin, J., 2022. Dudocaf: Dual-domain cross-attention fusion with recurrent transformer for fast multi-contrast mr imaging. In: International Conference on Medical Image Computing and Computer-Assisted Intervention. Springer, pp. 474–484.

Lyu, J., Wang, S., Tian, Y., Zou, J., Dong, S., Wang, C., Aviles-Rivero, A.I., Qin, J., 2024. STADNet: Spatial-temporal attention-guided dual-path network for cardiac cine MRI super-resolution. Med. Image Anal. 103142.

Ma, J., Zhang, Y., Gu, S., An, X., Wang, Z., Ge, C., Wang, C., Zhang, F., Wang, Y., Xu, Y., et al., 2022. Fast and low-GPU-memory abdomen CT organ segmentation: the flare challenge. Med. Image Anal. 82, 102616.

Martín-Isla, C., Campello, V.M., Izquierdo, C., Kushibar, K., Sendra-Balcells, C., Gkontra, P., Sojoudi, A., Fulton, M.J., Arega, T.W., Punithakumar, K., et al., 2023. Deep learning segmentation of the right ventricle in cardiac MRI: The M&ms challenge. IEEE J. Biomed. Heal. Inform..

Menchón-Lara, R.-M., Simmross-Wattenberg, F., Casaseca-de-la Higuera, P., Martín-Fernández, M., Alberola-López, C., 2019. Reconstruction techniques for cardiac cine MRI. Insights Into Imaging 10, 1–16.

Müller, T., Evans, A., Schied, C., Keller, A., 2022. Instant neural graphics primitives with a multiresolution hash encoding. ACM Trans. Graph. (ToG) 41 (4), 1–15.

Ouyang, C., Schlemper, J., Biffi, C., Seegoolam, G., Caballero, J., Price, A.N., Hajnal, J.V., Rueckert, D., 2019. Generalising deep learning MRI reconstruction across different domains. arXiv preprint arXiv:1902.10815.

Pan, J., Hamdi, M., Huang, W., Hammernik, K., Kuestner, T., Rueckert, D., 2024. Unrolled and rapid motion-compensated reconstruction for cardiac CINE MRI. Med. Image Anal. 91, 103017.

Petitjean, C., Zuluaga, M.A., Bai, W., Dacher, J.-N., Grosgeorge, D., Caudron, J., Ruan, S., Ayed, I.B., Cardoso, M.J., Chen, H.-C., et al., 2015. Right ventricle segmentation from cardiac MRI: a collation study. Med. Image Anal. 19 (1), 187–202.

Pontré, B., Cowan, B.R., DiBella, E., Kulaseharan, S., Likhite, D., Noorman, N., Tautz, L., Tustison, N., Wollny, G., Young, A.A., et al., 2016. An open benchmark challenge for motion correction of myocardial perfusion MRI. IEEE J. Biomed. Heal. Inform. 21 (5), 1315–1326.

Potlapalli, V., Zamir, S.W., Khan, S., Khan, F.S., 2023. PromptIR: Prompting for all-in-one blind image restoration. arXiv preprint arXiv:2306.13090.

Pruessmann, K.P., Weiger, M., Scheidegger, M.B., Boesiger, P., 1999. SENSE: sensitivity encoding for fast MRI. Magn. Reson. Med.: Off. J. Int. Soc. Magn. Reson. Med. 42 (5), 952–962.

Qi, H., Cruz, G., Botnar, R., Prieto, C., 2021. Synergistic multi-contrast cardiac magnetic resonance image reconstruction. Phil. Trans. R. Soc. A 379 (2200), 20200197.

Qin, C., Duan, J., Hammernik, K., Schlemper, J., Küstner, T., Botnar, R., Prieto, C., Price, A.N., Hajnal, J.V., Rueckert, D., 2021. Complementary time-frequency domain networks for dynamic parallel mr image reconstruction. Magn. Reson. Med. 86 (6), 3274–3291.

Qin, C., Rueckert, D., 2022. Artificial intelligence-based image reconstruction in cardiac magnetic resonance. In: Artificial Intelligence in Cardiothoracic Imaging. Springer, pp. 139–147.

Qin, C., Schlemper, J., Caballero, J., Price, A.N., Hajnal, J.V., Rueckert, D., 2018. Convolutional recurrent neural networks for dynamic MR image reconstruction. IEEE Trans. Med. Imaging 38 (1), 280–290.

Qin, C., Schlemper, J., Duan, J., Seegoolam, G., Price, A., Hajnal, J., Rueckert, D., 2019. k-t NEXT: dynamic MR image reconstruction exploiting spatio-temporal correlations. In: Medical Image Computing and Computer Assisted Intervention–MICCAI 2019: 22nd International Conference, Shenzhen, China, October 13–17, 2019, Proceedings, Part II 22. Springer, pp. 505–513.

Ronneberger, O., Fischer, P., Brox, T., 2015. U-net: Convolutional networks for biomedical image segmentation. In: Medical Image Computing and Computer-Assisted Intervention–MICCAI 2015: 18th International Conference, Munich, Germany, October 5-9, 2015, Proceedings, Part III 18. Springer, pp. 234–241.

Roy, S., Koehler, G., Ulrich, C., Baumgartner, M., Petersen, J., Isensee, F., Jäger, P.F., Maier-Hein, K.H., 2023. MedNeXt: Transformer-driven scaling of ConvNets for medical image segmentation. In: International Conference on Medical Image Computing and Computer-Assisted Intervention. Springer, pp. 405—-415.

Schlemper, J., Caballero, J., Hajnal, J.V., Price, A.N., Rueckert, D., 2017. A deep cascade of convolutional neural networks for dynamic MR image reconstruction. IEEE Trans. Med. Imaging 37 (2), 491–503.

Seegoolam, G., Schlemper, J., Qin, C., Price, A., Hajnal, J., Rueckert, D., 2019. Exploiting motion for deep learning reconstruction of extremely-undersampled dynamic MRI. In: International Conference on Medical Image Computing and Computer-Assisted Intervention. Springer, pp. 704–712.

Souza, R., Lucena, O., Garrafa, J., Gobbi, D., Saluzzi, M., Appenzeller, S., Rittner, L., Frayne, R., Lotufo, R., 2018. An open, multi-vendor, multi-field-strength brain MR dataset and analysis of publicly available skull stripping methods agreement. NeuroImage 170, 482–494.

Sriram, A., Zbontar, J., Murrell, T., Defazio, A., Zitnick, C.L., Yakubova, N., Knoll, F., Johnson, P., 2020. End-to-end variational networks for accelerated MRI reconstruction. In: Medical Image Computing and Computer Assisted Intervention–MICCAI 2020: 23rd International Conference, Lima, Peru, October 4–8, 2020, Proceedings, Part II 23. Springer, pp. 64–73.

Suinesiaputra, A., Ablin, P., Alba, X., Alessandrini, M., Allen, J., Bai, W., Cimen, S., Claes, P., Cowan, B.R., D'hooge, J., et al., 2017. Statistical shape modeling of the left ventricle: myocardial infarct classification challenge. IEEE J. Biomed. Heal. Inform. 22 (2), 503–515.

Suinesiaputra, A., Cowan, B.R., Al-Agamy, A.O., Elattar, M.A., Ayache, N., Fahmy, A.S., Khalifa, A.M., Medrano-Gracia, P., Jolly, M.P., Kadish, A.H., et al., 2014. A collaborative resource to build consensus for automated left ventricular segmentation of cardiac MR images. Med. Image Anal. 18 (1), 50–62.

Tänzer, M., Wang, F., Qiao, M., Bai, W., Rueckert, D., Yang, G., Nielles-Vallespin, S., 2023. T1/T2 relaxation temporal modelling from accelerated acquisitions using a latent transformer. In: International Workshop on Statistical Atlases and Computational Models of the Heart. Springer, pp. 293–302.

Tobon-Gomez, C., De Craene, M., Mcleod, K., Tautz, L., Shi, W., Hennemuth, A., Prakosa, A., Wang, H., Carr-White, G., Kapetanakis, S., et al., 2013. Benchmarking framework for myocardial tracking and deformation algorithms: An open access database. Med. Image Anal. 17 (6), 632–648.

Uecker, M., Lai, P., Murphy, M.J., Virtue, P., Elad, M., Pauly, J.M., Vasanawala, S.S., Lustig, M., 2014. ESPIRiT—an eigenvalue approach to autocalibrating parallel MRI: where SENSE meets GRAPPA. Magn. Reson. Med. 71 (3), 990–1001.

Vaswani, A., Shazeer, N., Parmar, N., Uszkoreit, J., Jones, L., Gomez, A.N., Kaiser, L., Polosukhin, I., 2017. Attention is all you need. In: Advances in Neural Information Processing Systems. pp. 5998–6008.

Wang, S., Ke, Z., Cheng, H., Jia, S., Ying, L., Zheng, H., Liang, D., 2022a. DIMENSION: dynamic MR imaging with both k-space and spatial prior knowledge obtained via multi-supervised network training. NMR Biomed. 35 (4), e4131.

Wang, C., Li, Y., Lv, J., Jin, J., Hu, X., Kuang, X., Chen, W., Wang, H., 2021. Recommendation for cardiac magnetic resonance imaging-based phenotypic study: imaging part. Phenomics 1, 151–170.

Wang, C., Lyu, J., Wang, S., Qin, C., Guo, K., Zhang, X., Yu, X., Li, Y., Wang, F., Jin, J., et al., 2023a. CMRxRecon: an open cardiac MRI dataset for the competition of accelerated image reconstruction. arXiv preprint arXiv:2309.10836.

Wang, Z., Qian, C., Guo, D., Sun, H., Li, R., Zhao, B., Qu, X., 2023b. One-dimensional deep low-rank and sparse network for accelerated MRI. IEEE Trans. Med. Imaging 42 (1), 79–90.

Wang, S., Qin, C., Wang, C., Wang, K., Wang, H., Chen, C., Ouyang, C., Kuang, X., Dai, C., Mo, Y., et al., 2022b. The extreme cardiac MRI analysis challenge under respiratory motion (CMRxMotion). arXiv preprint arXiv:2210.06385.

Wang, Z., Xiao, M., Zhou, Y., Wang, C., Wu, N., Li, Y., Gong, Y., Chang, S., Chen, Y., Zhu, L., et al., 2024. Deep separable spatiotemporal learning for fast dynamic cardiac MRI. arXiv preprint arXiv:2402.15939.

Wang, Z., Yu, X., Wang, C., Chen, W., Wang, J., Chu, Y.H., Sun, H., Li, R., Li, P., Yang, F., et al., 2023c. One for multiple: Physics-informed synthetic data boosts generalizable deep learning for fast MRI reconstruction. arXiv preprint arXiv:2307.13220.

Xie, Y., Li, Q., 2022. Measurement-conditioned denoising diffusion probabilistic model for under-sampled medical image reconstruction. In: International Conference on Medical Image Computing and Computer-Assisted Intervention. Springer, pp. 655–664.

Xin, B., Ye, M., Axel, L., Metaxas, D.N., 2023. Fill the k-space and refine the image: Prompting for dynamic and multi-contrast MRI reconstruction. In: International Workshop on Statistical Atlases and Computational Models of the Heart. Springer, pp. 261–273.

Xiong, Z., Xia, Q., Hu, Z., Huang, N., Bian, C., Zheng, Y., Vesal, S., Ravikumar, N., Maier, A., Yang, X., et al., 2021. A global benchmark of algorithms for segmenting the left atrium from late gadolinium-enhanced cardiac magnetic resonance imaging. Med. Image Anal. 67, 101832.

Yang, Q., Wang, Z., Guo, K., Cai, C., Qu, X., 2023. Physics-driven synthetic data learning for biomedical magnetic resonance: The imaging physics-based data synthesis paradigm for artificial intelligence. IEEE Signal Process. Mag. 40 (2), 129–140.

Yang, Z., Zhu, L., Wu, Y., Yang, Y., 2020. Gated channel transformation for visual recognition. In: Proceedings of the IEEE/CVF Conference on Computer Vision and Pattern Recognition. pp. 11794–11803.

Yiasemis, G., Moriakov, N., Sonke, J.-J., Teuwen, J., 2025. vSHARP: variable splitting half-quadratic admm algorithm for reconstruction of inverse-problems. Magn. Reson. Imaging 115, 110266.

Yiasemis, G., Sánchez, C.I., Sonke, J.-J., Teuwen, J., 2024. On retrospective k-space subsampling schemes for deep mri reconstruction. Magn. Reson. Imaging.

Yiasemis, G., Sonke, J.J., Sánchez, C., Teuwen, J., 2022. Recurrent variational network: A deep learning inverse problem solver applied to the task of accelerated MRI reconstruction. In: Proceedings of the IEEE/CVF Conference on Computer Vision and Pattern Recognition. CVPR, pp. 732–741.

Ying, L., Sheng, J., 2007. Joint image reconstruction and sensitivity estimation in SENSE (JSENSE). Magn. Reson. Med.: Off. J. Int. Soc. Magn. Reson. Med. 57 (6), 1196–1202.

Zbontar, J., Knoll, F., Sriram, A., Murrell, T., Huang, Z., Muckley, M.J., Defazio, A., Stern, R., Johnson, P., Bruno, M., et al., 2018. fastMRI: An open dataset and benchmarks for accelerated MRI. arXiv preprint arXiv:1811.08839.

Zhang, L., Chen, W., 2023. k-t CLAIR: Self-consistency guided multi-prior learning for dynamic parallel MR image reconstruction. In: International Workshop on Statistical Atlases and Computational Models of the Heart. Springer, pp. 314–325.

Zhang, L., Li, X., Chen, W., 2023a. CAMP-net: Consistency-aware multi-prior network for accelerated MRI reconstruction. arXiv preprint arXiv:2306.11238.

Zhang, M., Wu, Y., Zhang, H., Qin, Y., Zheng, H., Tang, W., Arnold, C., Pei, C., Yu, P., Nan, Y., et al., 2023b. Multi-site, multi-domain airway tree modeling. Med. Image Anal. 90, 102957.

Zhuang, X., Li, L., Payer, C., Štern, D., Urschler, M., Heinrich, M.P., Oster, J., Wang, C., Smedby, Ö., Bian, C., et al., 2019. Evaluation of algorithms for multi-modality whole heart segmentation: an open-access grand challenge. Med. Image Anal. 58, 101537.

Zhuang, X., Xu, J., Luo, X., Chen, C., Ouyang, C., Rueckert, D., Campello, V.M., Lekadir, K., Vesal, S., RaviKumar, N., et al., 2022. Cardiac segmentation on late gadolinium enhancement MRI: a benchmark study from multi-sequence cardiac MR segmentation challenge. Med. Image Anal. 81, 102528.